Supporting Information for

Trimesityltriangulene: A Persistent Derivative of Clar's Hydrocarbon

Leoš Valenta, Maximilian Mayländer, Pia Kappeler, Olivier Blacque, Tomáš Šolomek,* Sabine Richert,* and Michal Juríček*

Table of contents

S1. Supporting figures

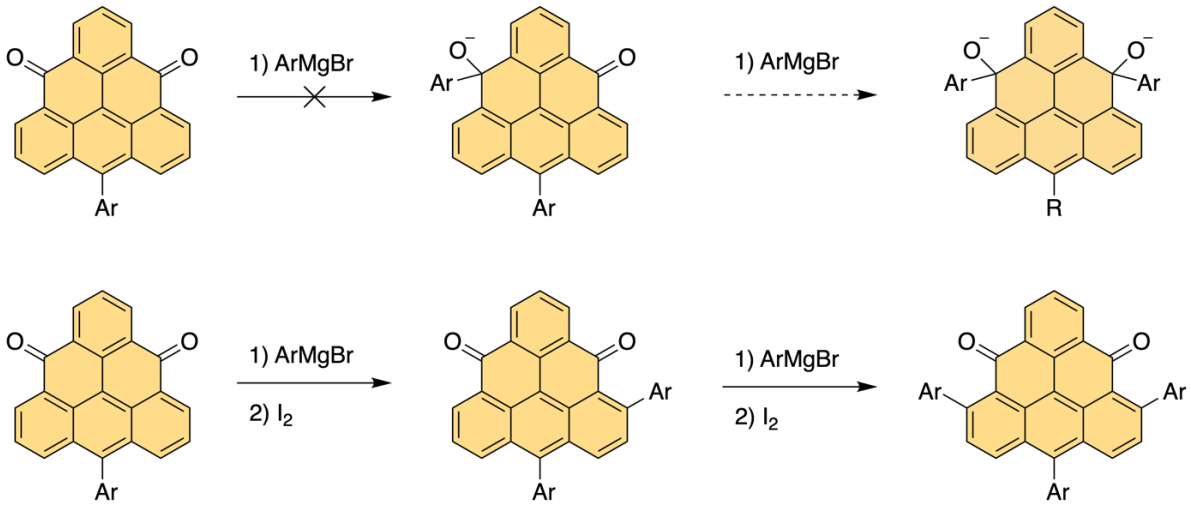

Fig. S1. First attempt. An attempt to prepare a trisubstituted triangulene precursor via a nucleophilic addition of a Grignard reagent to monoarylated triangulene-4,8-dione, readily available from a hydroxy derivative developed by Clar (top). Unexpectedly, a 1,4-addition instead of the desired 1,2-addition to the ketone occurred (bottom). Even though a trisubstituted derivative could be obtained using this method, the installment of the fourth substituent led to an sp^3 center, which impeded further transformations towards persistent triangulene.[1]

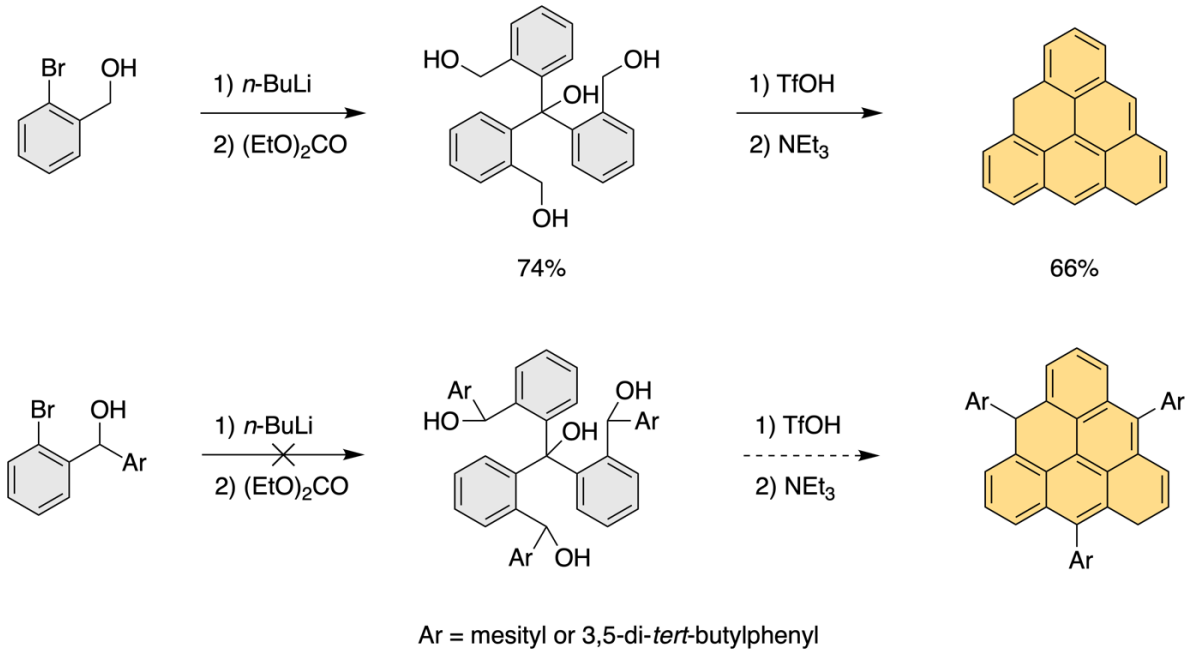

Fig. S2. Second attempt. A method reported by Johnson et al. for the synthesis of the dihydro-precursor of triangulene involving a three-fold ring-closure of a pre-functionalized precursor to dihydro-triangulene[2] (top). Our attempt to prepare a tetrahydroxy precursor for the acid-catalyzed ring-closure was not successful, most likely due to the crowdedness during the formation of the desired tetraol to synthesize a trisubstituted triangulene precursor (bottom).

UV–vis sample preparation. A mixture of **1a** + **1b** (2.4 mg, 3.8 μmol) and *p*-chloranil (4.6 mg, 19 μmol, 5 equivalents) were placed into a Schlenk tube and the atmosphere was exchanged three times with nitrogen. Then, toluene (1.5 mL) deoxygenated by freeze-pump-thaw technique in three cycles was added. For the measurements, an aliquot sample (30 μL) was diluted with deoxygenated toluene (3.0 mL) to a concentration of 2.5×10^{-5} M in an argon-flushed fluorescence cuvette equipped with a septum.

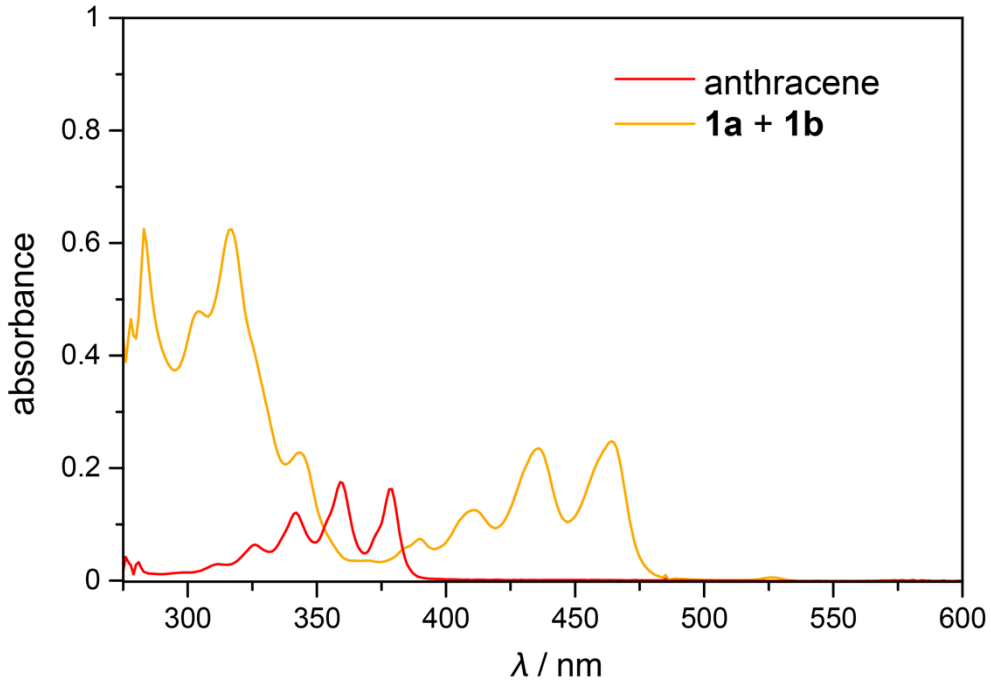

Fig. S3. Anthracene vibronic progression. UV–vis spectra for toluene solutions of anthracene and **1a** + **1b** (both 2.5×10^{-5} M).

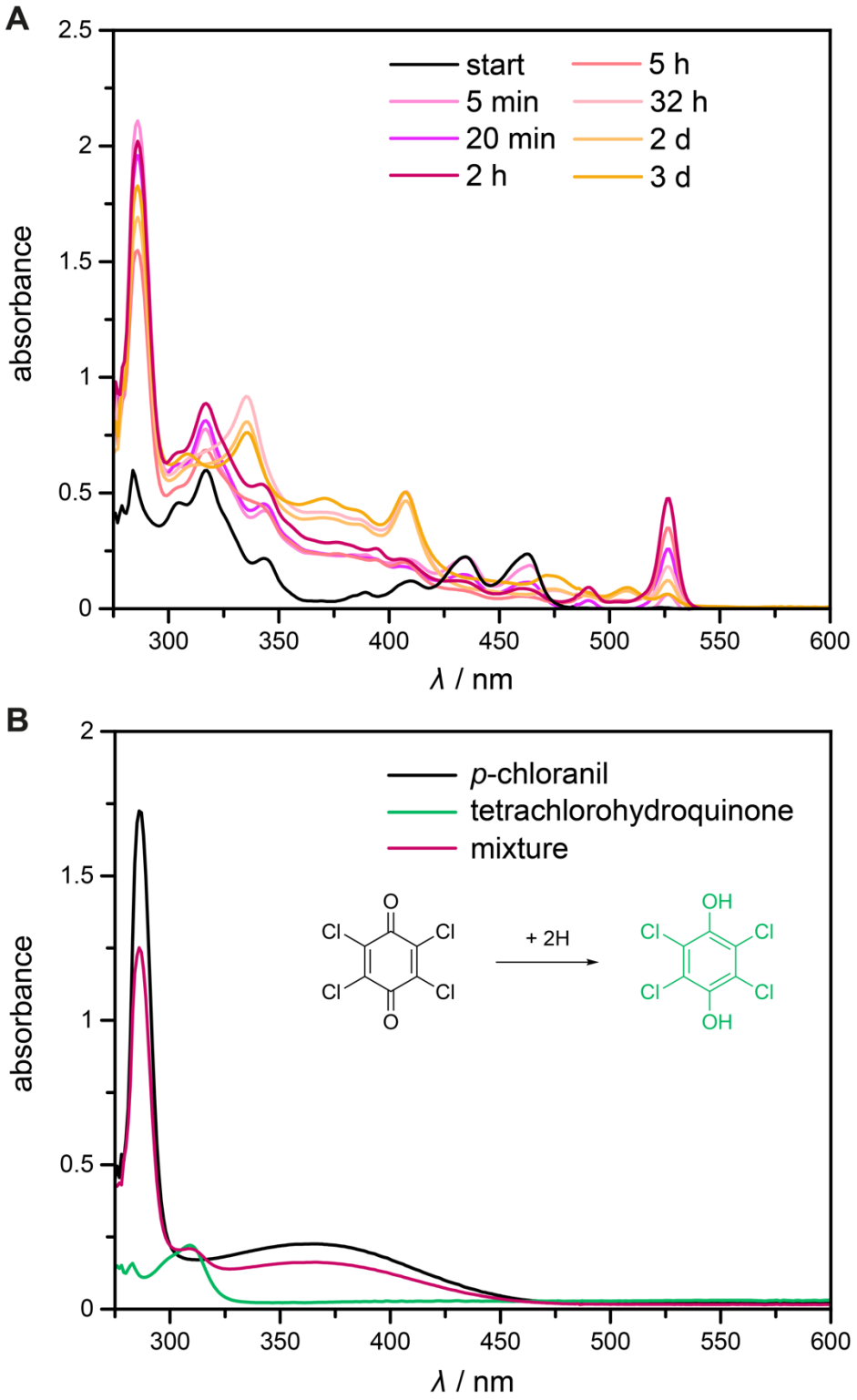

Fig. S4. Reaction monitoring. (A) UV–vis spectra for toluene solutions of a mixture of **1a** + **1b** with 5 equivalents of *p*-chloranil recorded before and after the oxidant addition (as indicated). The oxidation was performed at 2.5 mM concentration. For the UV–vis measurements, an aliquot sample of this solution was diluted to 2.5×10^{-5} M.

(B) UV–vis spectra for toluene solutions of *p*-chloranil (1.25×10^{-4} M), its reduced form (2.5×10^{-5} M) and a 4:1 mixture of *p*-chloranil and reduced *p*-chloranil (tetrachlorohydroquinone).

S2. General information

Anhydrous solvents and chemical reagents were purchased from commercial sources and used without further purification unless stated otherwise. The silica-gel column chromatography was performed using Merck 60 silica gel (40–63 μm). (2,6-Bis(methoxymethyl)phenyl)boronic acid was prepared according to the literature.[3,4] The NMR experiments were performed on NMR spectrometers operating at 400, 500 or 600 MHz proton frequencies. Standard pulse sequences were used. Chemical shifts (δ) are reported in parts per million (ppm) relative to the solvent residual peak[5] (^{1}H and ^{13}C NMR, respectively): $CDCl_3$ (δ = 7.26 and 77.16 ppm), CD_2Cl_2 (δ = 5.32 and 53.84 ppm). High-resolution mass spectra (HRMS) were measured as HR-ESI-MS, HR-APCI-MS or HR-EI-MS.

S3. Synthesis and characterization

2 **9**

9-Mesitylanthracene (9). A solution of 2-mesitylmagnesium bromide (4.1 mL, 4.1 mmol, 1.0 M in THF) was added to a solution of anthrone (500 mg, 2.57 mmol) in dry THF (20 mL) under a nitrogen atmosphere. The reaction mixture was stirred at 65 °C for 3 h before conc. HCl (4.3 mL) was added and the reaction mixture was stirred overnight at 65 °C. The mixture was extracted with DCM (3 × 30 mL). The combined organic layers were washed with brine, dried over anhydrous $MgSO_4$ and filtered. After evaporation of the solvents, the residue was purified by column chromatography (SiO_2, cyclohexane/ethyl acetate, 50:1) to afford the product (240 mg, 32%) as a white solid. ^{1}H NMR (400 MHz, $CDCl_3$, ppm): δ 8.51 (s, 1H), 8.09 (d, J = 8.5 Hz, 2H), 7.53 (d, J = 8.8 Hz, 2H), 7.49 (ddd, J = 8.1, 6.4, 1.2 Hz, 2H), 7.36 (ddd, J = 8.3, 6.5, 1.3 Hz, 2H), 7.14 (s, 2H), 2.50 (s, 3H), 1.76 (s, 6H). ^{13}C NMR (101 MHz, $CDCl_3$, ppm): δ 137.7, 137.2, 135.9, 134.6, 131.8, 129.9, 128.8, 128.4, 126.2, 126.1, 125.7, 125.3, 21.4, 20.1. This compound was prepared previously using a different procedure. The NMR data are in agreement with those reported.[6]

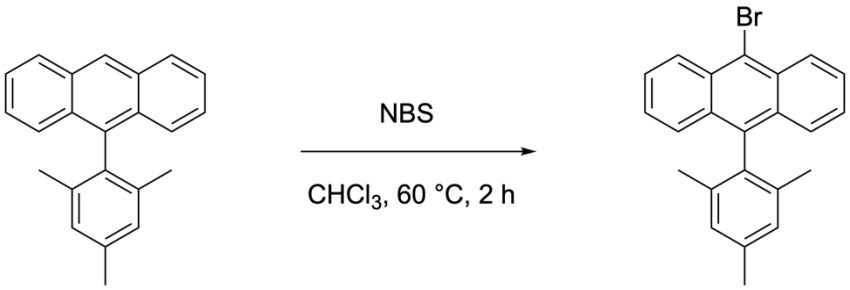

9 **3**

9-Bromo-10-mesitylanthracene (3). *N*-Bromsuccinimide (NBS; 613 mg, 3.44 mmol) was added in one portion to a solution of **9** (850 mg, 2.87 mmol) in $CHCl_3$ (30 mL) and the reaction mixture was stirred at 60 °C for 2 h. Upon cooling to room temperature, water (40 mL) was added and the mixture was extracted with DCM (3 × 50 mL). The combined organic phases were dried over $MgSO_4$ and the solvent was evaporated. The residue was purified by column chromatography (SiO_2, cyclohexane) to afford the product (790 mg, 73%) as a pale yellow solid. ^{1}H NMR (400 MHz, $CDCl_3$, ppm): δ 8.64 (d, J = 8.9 Hz, 2H), 7.60 (ddd, J = 8.8, 6.5, 1.3 Hz, 2H), 7.52 (d, J = 8.7 Hz, 2H), 7.37 (ddd, J = 8.8, 6.5, 1.2 Hz, 2H), 7.11 (s, 2H), 2.47 (s, 3H), 1.72 (s, 6H). ^{13}C NMR (101 MHz, $CDCl_3$, ppm): δ 137.60, 137.56, 136.7, 134.2, 130.7, 130.6, 128.5, 128.2, 127.2, 126.5, 126.0, 122.4, 21.4, 20.1. This compound was prepared previously using a similar procedure. The NMR data are in agreement with those reported.[7]

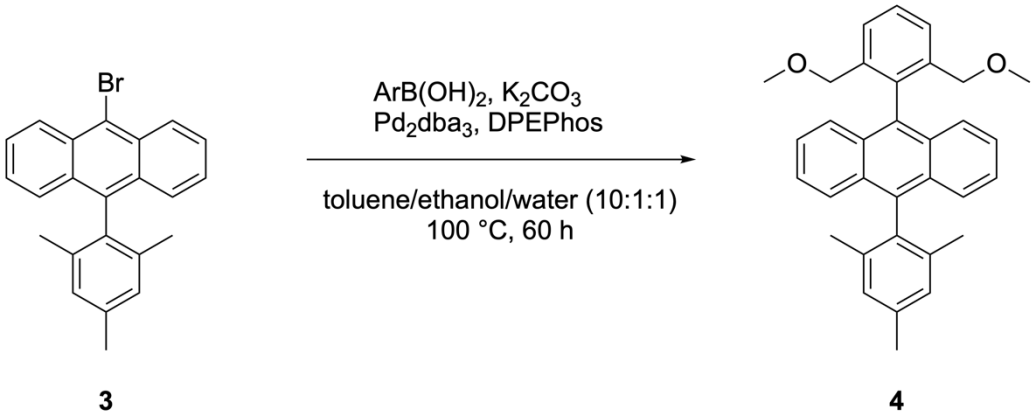

3 **4**

9-(2,6-Bis(methoxymethyl)phenyl)-10-mesitylanthracene (4). A mixture of **3** (563 mg, 1.50 mmol), (2,6-bis(methoxymethyl)phenyl)boronic acid (600 mg, 2.85 mmol), DPEPhos (81 mg, 0.15 mmol), Pd_2dba_3 (69 mg, 0.075 mmol) and K_2CO_3 (1.2 g, 9.0 mmol) in toluene (20 mL), ethanol (2 mL) and water (2 mL) was deoxygenated in a Schlenk flask by freeze-pump-thaw technique in three cycles and then stirred at 100 °C for 60 h. Upon cooling to room temperature, water (30 mL) was added and the mixture was extracted with DCM (3 × 20 mL). The combined

organic phases were dried over $MgSO_4$ and the solvent was evaporated. The residue was purified by column chromatography (SiO_2, cyclohexane/ethyl acetate, 25:1) to afford the product (383 mg, 55%) as an off-white solid. ^{1}H NMR (500 MHz, $CDCl_3$, ppm): δ 7.68 (2 × d, avg. J = 7.5 Hz, 2H), 7.63 (dd, J = 8.7, 6.5 Hz, 1H), 7.56–7.51 (m, 2H), 7.48–7.44 (m, 2H), 7.34–7.28 (m, 4H), 7.13 (s, 2H), 3.87 (s, 4H), 2.95 (s, 6H), 2.48 (s, 3H), 1.78 (s, 6H). ^{13}C NMR (126 MHz, $CDCl_3$, ppm): δ 138.4, 137.6, 137.4, 136.4, 135.6, 134.8, 131.9, 130.1, 129.6, 128.52, 128.46, 126.6, 126.5, 126.4, 125.7, 125.6, 72.2, 58.4, 21.4, 20.1. HRMS (ESI) *m/z*: [M + Na]$^+$ Calcd for $C_{33}H_{32}O_2$ 483.22945; Found 483.22931.

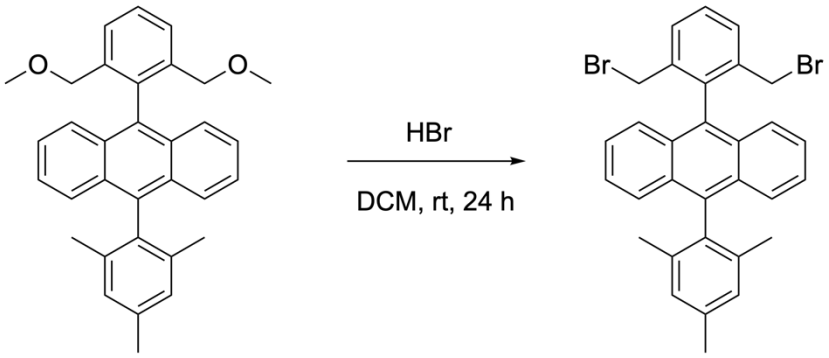

4 **5**

9-(2,6-Bis(bromomethyl)phenyl)-10-mesitylanthracene (5). Compound **4** (300 mg, 0.651 mmol) was placed into flame-dried Schlenk flask and the atmosphere was exchanged three times with nitrogen before dry DCM (4 mL) was added. To this solution, HBr (1.2 mL, 6.5 mmol, 33% in acetic acid) was added and the reaction mixture was stirred at room temperature for 24 h. The mixture was poured into water and extracted with DCM (3 × 20 mL). The combined organic phases were dried over $MgSO_4$ and the solvent was evaporated. The residue was purified by column chromatography (SiO_2, cyclohexane/ethyl acetate, 40:1) to afford the product (250 mg, 69%) as a white solid. ^{1}H NMR (400 MHz, $CDCl_3$, ppm): δ 7.74 (2 × d, avg. J = 7.7 Hz, 2H), 7.62 (dd, J = 8.3, 7.1 Hz, 1H), 7.57 (ddd, J = 6.7, 4.0, 2.0 Hz, 2H), 7.47–7.41 (m, 2H), 7.38–7.31 (m, 4H), 7.14 (s, 2H), 4.02 (s, 4H), 2.49 (s, 3H), 1.80 (s, 6H). ^{13}C NMR (101 MHz, $CDCl_3$, ppm): δ 138.3, 138.2, 137.6, 137.5, 137.4, 134.6, 131.2, 130.4, 130.0, 129.7, 129.4, 128.5, 126.7, 126.5, 126.0, 125.8, 31.4, 21.4, 20.1. HRMS (EI) *m/z*: [M]$^+$ Calcd for $C_{31}H_{26}Br_2$ 556.03958; Found 556.03945.

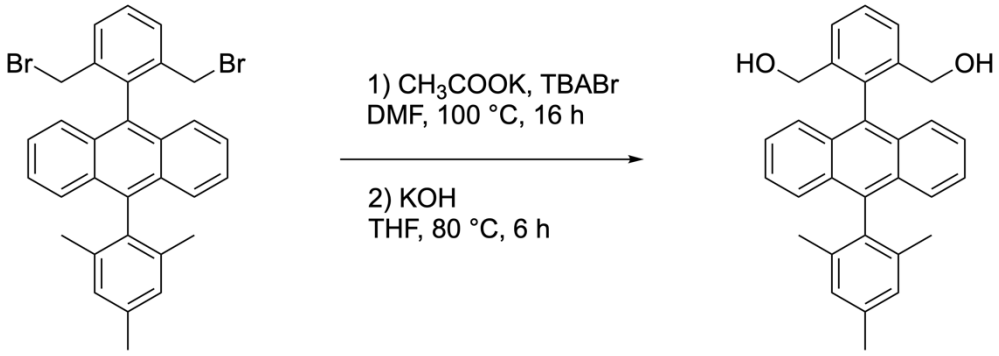

5 **6**

(2-(10-Mesitylanthracen-9-yl)-1,3-phenylene)dimethanol (6). A solution of **5** (250 mg, 0.448 mmol), potassium acetate (440 mg, 4.48 mmol) and tetrabutylammonium bromide (144 mg, 0.448 mmol) in DMF (5 mL) was stirred at 100 °C for 16 h under a nitrogen atmosphere. Upon cooling, the reaction mixture was poured over ice and extracted with DCM (3 × 15 mL). The combined organic phases were extracted twice with an excess of water, aq. LiCl (5%) and then dried over $MgSO_4$. The crude pale yellow oil was dissolved in THF (4 mL) and added to a solution of KOH (252 mg, 4.50 mmol) in ethanol (4 mL) and water (2 mL), and the mixture was stirred at 80 °C for 6 h. Then, sat. NH_4Cl (10 mL) was added and the mixture was extracted with DCM (3 × 15 mL). The combined organic phases were dried over $MgSO_4$ and the solvent was evaporated. The residue was purified by column chromatography (SiO_2, cyclohexane/ethyl acetate, 3:1) to afford the product (190 mg, 98% over two steps) as a pale yellow solid. ^{1}H NMR (400 MHz, $CDCl_3$, ppm): δ 7.74 (2 × d, avg. J = 7.6 Hz, 2H), 7.68 (dd, J = 8.7, 6.4 Hz, 1H), 7.58–7.52 (m, 2H), 7.49–7.43 (m, 2H), 7.37–7.29 (m, 4H), 7.13 (s, 2H), 4.14 (s, 4H), 2.48 (s, 3H), 1.77 (s, 6H).^{13}C NMR (101 MHz, $CDCl_3$, ppm): δ 140.6, 137.6, 137.5, 137.0, 135.1, 134.5, 131.3, 130.1, 129.7, 129.1, 128.5, 127.1, 126.8, 126.5, 125.82, 125.79, 63.3, 21.4, 20.2. HRMS (ESI) *m/z*: $[M + Na]^+$ Calcd for $C_{31}H_{28}O_2$ 455.19815; Found 455.19794.

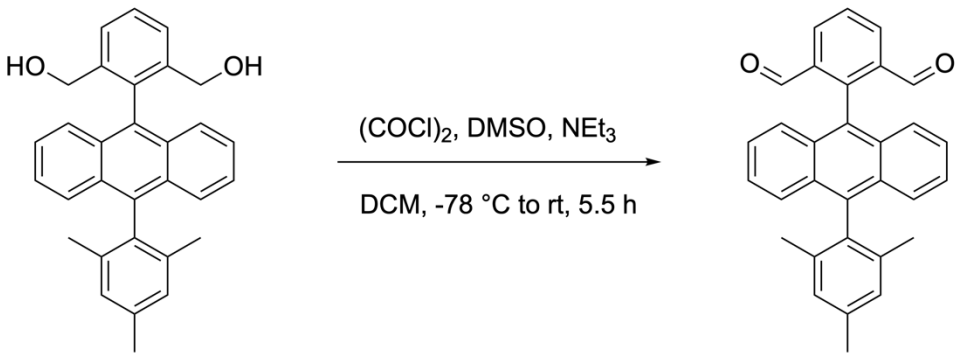

6 **7**

2-(10-Mesitylanthracen-9-yl)isophthalaldehyde (7). To a cooled (–78 °C) mixture of oxalyl chloride (0.12 mL, 1.4 mmol) in dry DCM (5 mL), DMSO (0.2 mL, 3 mmol) was added dropwise and the mixture was stirred at –78 °C for 30 min before a solution of **6** (195 mg, 0.451 mmol) in dry DCM (8 mL) was added. The reaction mixture was stirred at –78 °C for 1 h, then triethylamine (3.75 mL, 27.0 mmol) was added dropwise and the mixture was stirred at –78 °C for 2 h and then at room temperature for 2 h. The mixture was quenched by the addition of aq. HCl (10 mL, 1 M) and extracted with DCM (3 × 10 mL). The combined organic phases were dried over $MgSO_4$ and the solvent was evaporated. The residue was purified by column chromatography (SiO_2, DCM/cyclohexane, 3:1) to afford the product (150 mg, 78%) as a yellow solid. ^{1}H NMR (400 MHz, $CDCl_3$, ppm): δ 9.32 (s, 2H), 8.50 (d, J = 7.7 Hz, 2H), 7.89 (t, J = 7.7 Hz, 1H), 7.64–7.58 (m, 2H), 7.45–7.33 (m, 6H), 7.14 (s, 2H), 2.49 (s, 3H), 1.78 (s, 6H). ^{13}C NMR (101 MHz, $CDCl_3$, ppm): δ 190.9, 146.2, 138.8, 137.8, 137.5, 136.4, 134.0, 133.1, 131.9, 129.3, 129.2, 128.6, 127.3, 126.9, 126.1, 126.0, 125.2, 21.4, 20.2. HRMS (ESI) *m/z*: $[M + H]^+$ Calcd for $C_{31}H_{24}O_2$ 429.18491; Found 429.18557.

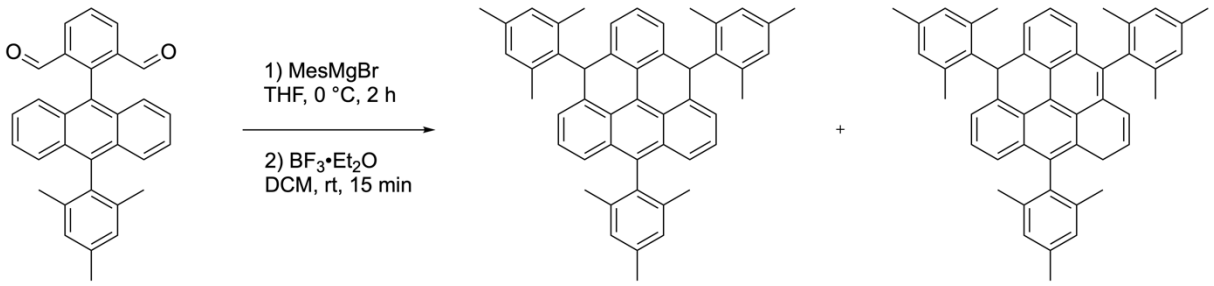

7 **1a** **1b**

4,8,12-Trimesityl-4,8-dihydrodibenzo[*cd*,*mn*]pyrene (1a) + 4,8,12-trimesityl-1,8-dihydrodibenzo[*cd*,*mn*]pyrene (1b). To a cooled (0 °C) solution of **7** in dry THF (3 mL), 2-mesitylmagnesium bromide (0.47 mL, 0.47 mmol, 1.0 M in THF) was added dropwise and the reaction mixture was allowed to warm to room temperature and then it was stirred for additional 2 h. The mixture was quenched by the addition of water (5 mL) and then extracted with DCM (3 × 5 mL). The combined organic phases were dried over Na_2SO_4 and the solvent was evaporated. The oily residue was heated to 35 °C and kept under high vacuum for 24 h in order to remove all residual mesitylene. The crude dihydroxy intermediate was used in the next step without further purification. It was dissolved in dry DCM (10 mL) and deoxygenated by freeze-pump-thaw technique in three cycles before BF_3•Et_2O (73 μL, 0.28 mmol) was added slowly. The reaction mixture was stirred at room temperature for 15 min, then quenched by the addition of cold deoxygenated methanol (0.5 mL). The solvent was evaporated using a Schlenk line and

the residue was purified by column chromatography (SiO_2, cyclohexane/DCM, 3:1) under inert conditions using deoxygenated silica gel and solvent (see image on the right). A yellow fluorescent compound was collected into a Schlenk flask and the solvent was evaporated using a Schlenk line. The product (24 mg, 81%), which is a pale yellow solid, was obtained as a mixture of two structural isomers **1a** and **1b**, where isomer **1a** is present as a mixture of two stereoisomers *syn*-**1a** and *anti*-**1a** (for structures, see Section S7). Because of significant overlap in the aromatic region, ^{1}H NMR spectrum cannot be fully described. However, analysis of the spectrum using the characteristic signals (6.42 (s, 2H, *syn*-**1a**), 6.37 (s, 2H, *anti*-**1a**), 6.60 (s, 1H, **1b**), 6.24 (dt, J = 10.0, 2.2 Hz, 1H, **1b**), 5.97 (dt, J = 10.1, 4.0 Hz, 1H, **1b**), 3.46 (dd, J = 4.1, 2.3 Hz, 2H, **1b**)) allowed us to estimate the composition of the mixture: *syn*-**1a**/*anti*-**1a**/**1b** ~ 1:0.4:1. Considering the rate of rotation of the mesityl groups relative to the NMR time-scale (3 × slow for *syn*-**1a**, 3 × fast for *anti*-**1a**, 2 × slow and 1 × fast for **1b**), 18 methyl (Me) resonances are expected, which matches well the observation (18 Me signals in ^{1}H and 17 in ^{13}C NMR). Considering the isomeric ratio, the aromatic signals should integrate to roughly 35H, which also matches well the observation. In addition, all 80 expected ^{13}C NMR signals in the aromatic region are visible. For details, see Section S7.

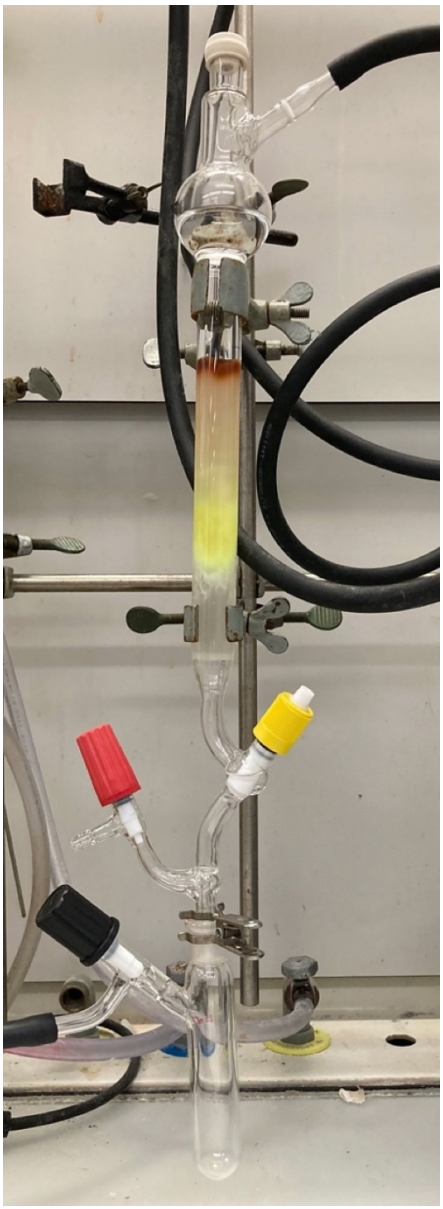

^{13}C NMR (151 MHz, CD_2Cl_2, ppm): δ 142.43, 142.24, 141.90, 138.43, 138.39, 138.37, 138.22, 137.98, 137.96, 137.89, 137.79, 137.75, 137.70, 137.65, 137.58, 137.54, 137.51, 137.42, 137.40, 137.39, 137.09, 136.66, 136.64, 136.59, 136.34, 136.32, 135.89, 135.84, 135.75, 135.62, 135.55, 135.52, 135.22, 132.91, 131.67, 131.64, 131.62, 131.40, 130.80, 130.24, 130.16, 129.87, 129.37, 129.28, 129.26, 129.03, 129.01, 128.87, 128.71, 128.70, 128.68, 128.66, 128.65, 128.59, 128.57, 128.50, 128.44, 127.97, 127.81, 127.23, 127.10, 126.98, 126.34, 126.26, 126.18, 126.15, 125.44, 125.09, 125.05, 124.66, 124.45, 124.25, 123.98, 123.89, 123.77, 123.71, 123.61, 123.58, 123.26, 122.62, 44.19, 44.05, 43.80, 30.10, 21.43, 21.34, 21.33, 21.30, 21.26, 21.04, 21.01, 20.64, 20.57, 20.23, 20.20, 20.07, 20.02, 19.97, 19.80, 19.79, 19.73. HRMS (APCI) *m/z*: $[M + H]^+$ Calcd for $C_{49}H_{44}$ 633.34430; Found 633.35148.

S4. X-ray crystallography

Table S1. Crystal data for 8a

CCDC no.	2104838
Empirical formula	$C_{51.5}H_{49}$
Formula weight	667.90
Temperature / K	160(1)
Crystal system	triclinic
Space group	P-1
a / Å	13.0757(6)
b / Å	17.7775(8)
c / Å	18.1806(8)
α / °	80.129(4)
β / °	70.657(4)
γ / °	89.633(4)
Volume / Å^3	3922.8(3)
Z	4
ρ_{calc} / g cm^{-3}	1.131
μ / mm^{-1}	0.475
F(000)	1432.0
Crystal size / mm^3	0.14 × 0.06 × 0.02
Radiation	Cu Kα (λ = 1.54184)
2Θ range for data collection / °	5.236 to 149.006
Index ranges	$-16 \le h \le 16$, $-22 \le k \le 22$, $-22 \le l \le 22$
Reflections collected	73678
Independent reflections	16006 [R_{int} = 0.0755, R_{sigma} = 0.0556]
Data/restraints/parameters	16006/144/901
Goodness-of-fit on F^2	1.033
Final *R* indexes [$I \ge 2\sigma(I)$]	R_1 = 0.0840, wR_2 = 0.2320
Final *R* indexes [all data]	R_1 = 0.1293, wR_2 = 0.2680
Largest diff. peak/hole / e Å^{-3}	0.43/–0.31

X-ray diffraction. Single-crystal X-ray diffraction data were collected at 160(1) K on a Rigaku OD Synergy/Pilatus detector diffractometer using Cu K_α radiation (λ = 1.54184 Å) from a micro-focus X-ray source and an Oxford Instruments Cryojet XL cooler. The selected suitable single crystal was mounted using polybutene oil on a flexible loop fixed on a goniometer head and immediately transferred to the diffractometer. Pre-experiment, data collection, data reduction and analytical absorption correction[8] were performed with the program suite *CrysAlisPro*.[9] Using *Olex2*,[10] the structure was solved with the SHELXT[11] small molecule structure solution program and refined with the *SHELXL2018/3* program package[12] by full-matrix least-squares minimization on F.[9] *PLATON*[13] was used to check the result of the X-ray analysis. For more details about the data collection and refinement parameters, see the CIF file. A solvent mask[14] was calculated and 123 electrons corresponding to solvent molecules were found per unit cell. We considered one molecule of pentane per asymmetric unit.

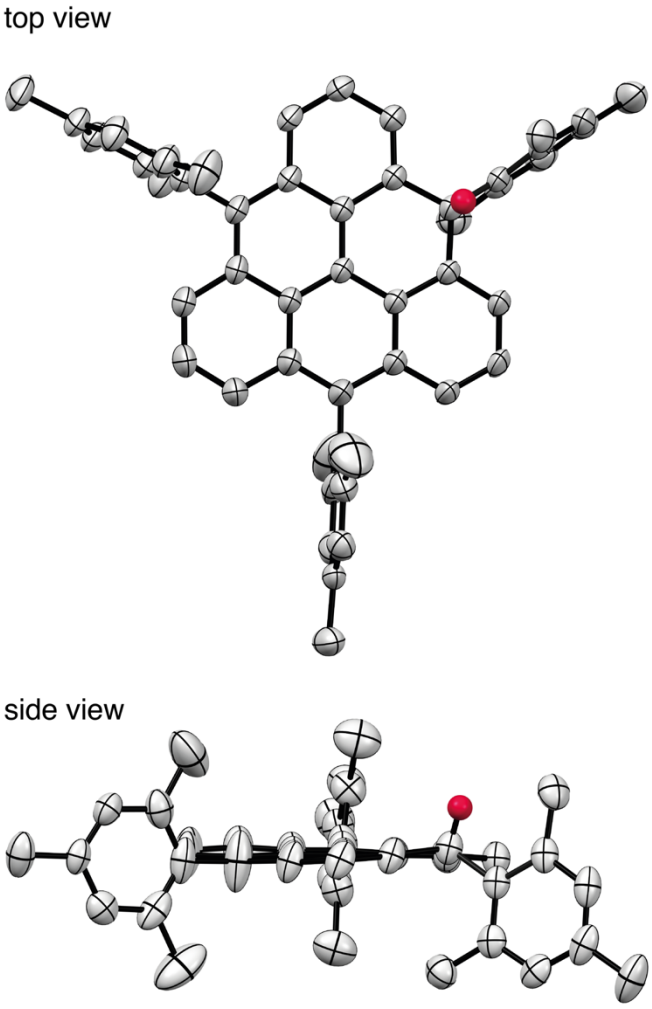

Fig. S5. Crystallographic characterization of triangulene monoradical. The solid-state structure of monoradical **8a**. Thermal ellipsoids are shown at the 50% probability level. The hydrogen atoms are omitted for clarity except for the C_{sp3} hydrogen atom highlighted in red. Crystals were obtained by slow evaporation of pentane under ambient conditions.

Table S2. Comparison of bond lengths obtained from XRD and DFT for 8a

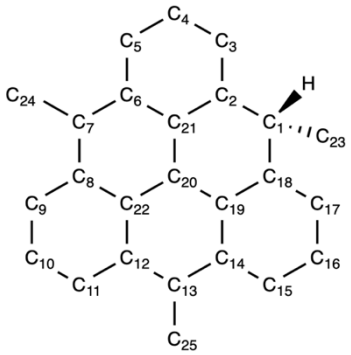

Bond	DFT / Å	XRD / Å
C_1–C_2	1.527	1.511
C_2–C_3	1.387	1.395
C_3–C_4	1.407	1.392
C_4–C_5	1.376	1.375
C_5–C_6	1.423	1.408
C_6–C_7	1.426	1.442
C_7–C_8	1.412	1.411
C_8–C_9	1.424	1.439
C_9–C_{10}	1.390	1.395
C_{10}–C_{11}	1.390	1.390
C_{11}–C_{12}	1.424	1.445
C_{12}–C_{13}	1.412	1.393
C_{13}–C_{14}	1.426	1.419
C_{14}–C_{15}	1.423	1.418
C_{15}–C_{16}	1.376	1.370
C_{16}–C_{17}	1.407	1.402
C_{17}–C_{18}	1.387	1.378
C_{18}–C_1	1.527	1.522
C_{18}–C_{19}	1.420	1.418
C_{19}–C_{14}	1.436	1.434
C_{19}–C_{20}	1.441	1.427
C_{20}–C_{21}	1.441	1.444
C_{20}–C_{22}	1.408	1.408
C_{21}–C_2	1.420	1.410
C_{21}–C_6	1.436	1.417
C_{22}–C_8	1.446	1.423
C_{22}–C_{12}	1.446	1.441
C_{23}–C_1	1.534	1.535
C_{24}–C_7	1.500	1.508
C_{25}–C_{13}	1.500	1.507
C_1–H	1.098	1.000

S5. EPR spectroscopy

EPR sample preparation. A mixture of **1a** + **1b** (0.4 mg, 0.6 μmol) and *p*-chloranil (0.8 mg, 3 μmol, 5 equivalents) were placed into separate vials with a screw-cap septum under ambient conditions. The septa were pierced with a needle and the vials were transferred into the glovebox, where *p*-chloranil was dissolved in deoxygenated toluene (250 μL) and then transferred into the vial with **1a** + **1b**. The reaction mixture was gently shaken, and after about 30 min the solution was transferred into a quartz EPR tube, which was then sealed with Critoseal®. Note that the described procedure applies to samples with a concentration of 2.5 mM. For different concentrations, the amount of solvent was adapted accordingly. For EPR measurements at the X- or Q-band, quartz EPR tubes with an outer diameter of 3.8 mm (inner diameter of ~3 mm, 125 μL of sample solution) or 1.6 mm (inner diameter of ~1 mm, 15 μL of sample solution), respectively, were used. For measurements at cryogenic temperatures, the EPR samples were rapidly frozen in liquid nitrogen before insertion into the EPR resonator.

Continuous wave EPR spectroscopy. X-band continuous wave EPR spectra were recorded on a Bruker EMXnano benchtop EPR spectrometer. The modulation frequency was set to 100 kHz and the modulation amplitude to 0.01 mT unless stated otherwise. The microwave power was adjusted for every sample to avoid saturation effects. At room temperature, a value of 0.063 mW (32 dB, 100 mW source) was found to be optimal, while much lower powers (0.0025 mW, corresponding to 46 dB) were necessary at 120 K. Room temperature cw EPR measurements at Q-band frequencies were performed on a Bruker ELEXSYS E580 spectrometer using an EN 5107D2 resonator. The modulation frequency was set to 50 kHz and the modulation amplitude to 0.03 mT (32 dB microwave attenuation). After data acquisition, all spectra were baseline-corrected, frequency-corrected to either 9.75 GHz (X-band) or 34.0 GHz (Q-band) and field-corrected using a carbon fiber standard with g = 2.002644.[15] The g value was calculated from the center of the experimental spectrum according to $g = \frac{h \cdot \nu}{\beta_e B_0}$ and further confirmed by numerical simulation of the spectra using EasySpin functions in MATLAB as detailed below.

Continuous wave EPR simulation procedure. For the simulations of the cw EPR spectra, the calculated hyperfine coupling constants from DFT (cf. Supporting Table S10) were taken as the basis. Only couplings larger than 0.5 MHz were considered as only these are resolved in the experimental spectra. An empirically determined scaling factor of 0.93 was applied to all calculated isotropic hyperfine coupling constants since this was found to yield the best

agreement with the experimental data. The application of a global scaling factor is also in line with the observation in the literature that hyperfine coupling constants computed by DFT are typically in good agreement with the experiment, but are frequently slightly overestimated.[16] The simulations were carried out using the EasySpin routine 'pepper' (instead of 'garlic'). This choice, unusual for the simulation of isotropic cw EPR spectra, was motivated by the fact that common simulation routines for fast motion EPR spectra rely on the Kivelson formulas (for anisotropic linewidths), implying that only systems with $S = 0.5$ can be accounted for. All calculated isotropic hyperfine couplings larger than 0.5 MHz were entered as computed by DFT (Table S10) and multiplied by the global scaling factor. The isotropic g value obtained from DFT was adapted slightly to best match the experimental spectrum and an appropriate linewidth (~0.03–0.04 mT) was chosen to account for unresolved hyperfine couplings. Since between 14 and 18 individual protons needed to be considered, it became computationally too expensive to treat all hyperfine couplings exactly using matrix diagonalization. Instead, matrix diagonalization was only applied for the nuclei with the six largest hyperfine couplings; all other nuclei were treated using perturbation theory, making use of the 'hybrid' method in EasySpin.

Comments on the continuous wave EPR simulations

Using the simulation procedure described above, a near perfect fit was obtained for the spectrum with 5 equivalents of the oxidant, leaving little doubt regarding the triplet nature of the triangulene diradical **Mes$_3$-Tr**. In contrast, the simulation of the spectrum with 0.1 equivalents turned out to be less straightforward. In that case, the simulation is complicated by the fact that two isomers **8a** and **8b** are thought to contribute significantly to the spectrum of the triangulene monoradical **8** and that the exact ratio of these two contributing species is unknown. In addition, also experimentally it is challenging to obtain a spectrum of 'pure' monoradical. Even if a very small amount of the oxidant was added (0.1 equivalents), we observed slightly different shapes of the cw EPR spectra when the experiment was repeated several times, suggesting that a small part of the molecules nevertheless undergoes further oxidation to the diradical. However, despite these complications, the agreement between simulation and experiment is surprisingly good, especially with respect to the magnitude of the hyperfine couplings and thus confirms our assignment.

Pulse EPR spectroscopy. The pulse EPR measurements were carried out on a Bruker ELEXSYS E580 spectrometer operated at the Q-band, equipped with an EN 5107D2 resonator.

During the measurement, the sample was kept at a constant temperature of 120 K, using an Oxford Instruments nitrogen gas-flow cryostat (CF 935).

Transient nutations. Transient nutation measurements used the microwave pulse sequence $\xi - \tau - \pi - \tau -$ echo where the flip angle ξ was gradually increased by increasing the corresponding microwave pulse length in steps of 2 ns, starting at 20 ns (i.e., $\frac{\pi}{2}$). At every magnetic field position within the region of the EPR spectrum, the integrated echo intensity was then recorded as a function of this pulse length. The magnetic field step size was set to 0.25 G (field scan range of 50 G, 200 points). The whole data set was background corrected using a polynomial background function. The (cross-term averaged) Fourier transform was then calculated after dead-time reconstruction, windowing using a Hamming window, and zero filling to 2000 data points. The frequency spectra were normalized by division of the frequency axis by the reference frequency obtained for a species with doublet multiplicity (**8a** and **8b**). The 2D-data set of the frequency spectra as a function of field is shown in Fig. 3.

Additional cw EPR data

On a sample of **1a** + **1b** with oxidant in toluene, room temperature cw EPR spectra were acquired at two different microwave frequencies (X and Q-band) to verify if additional features can be resolved in the spectra when the experiments are performed at higher microwave frequencies. These experiments were performed for 0.1 and 5 equivalents of the oxidant and are shown in Fig. S6. Since no significant differences in the spectral shape were observed, all further cw EPR spectra were recorded at X-band frequencies only.

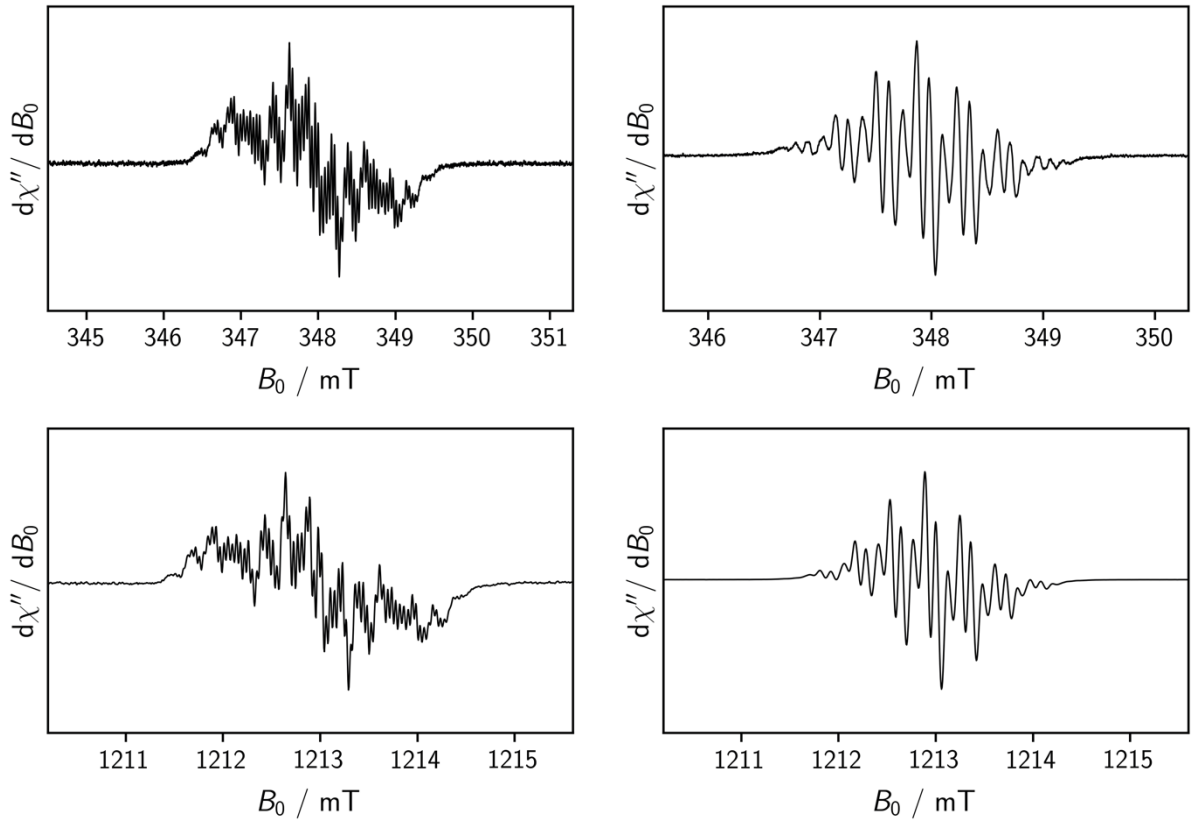

Fig. S6. Room temperature cw EPR spectra of a 2.5 mM solution of **1a** + **1b** in toluene with 0.1 (left) and 5 (right) equivalents of the oxidant recorded at X- (top) and Q-band (bottom) frequencies.

To find suitable conditions for pulse EPR experiments and verify the reproducibility of the data, cw EPR spectra were recorded using different concentrations of **1a** + **1b**, different oxidant equivalents and different waiting times after oxidant addition. It was found that the same spectrum is obtained when either (i) adding more of the oxidant and recording the spectrum shortly after oxidant addition or (ii) adding less oxidant and leaving the sample to react for a longer time. This behavior is expected for a chemical oxidation to the diradical **Mes$_3$-Tr** and underlines the reproducibility of the spectral shape. An exemplary data set is shown in Fig. S7. The 'best' spectrum for monoradical **8** could be obtained when using low concentrations of **1a** + **1b** ($\leq$ 0.5 mM) and oxidant equivalents lower or equal than one.

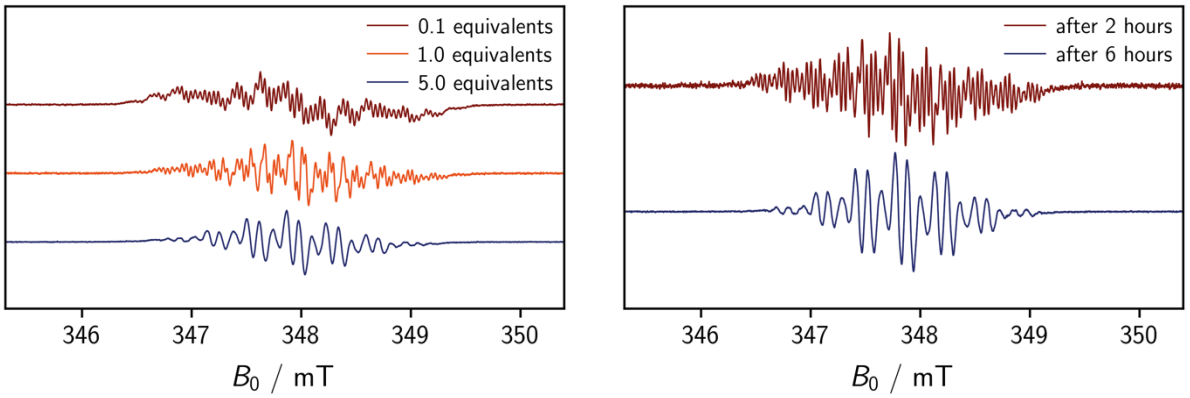

Fig. S7. Room temperature cw EPR spectra of a 1 mM solution of **1a** + **1b** in toluene at different oxidant concentrations (as indicated, left) and a 0.5 mM solution of **1a** + **1b** in toluene with 1 equivalent of the oxidant at different times after oxidant addition (as indicated, right).

Fig. S8 shows the cw EPR spectra for the samples of a 2.5 mM solution of **1a** + **1b** and oxidant in toluene that were used for the pulse EPR measurements (transient nutations). For these experiments, we deliberately employed only a short waiting time after oxidant addition since we did not want the monoradical species **8** to react any further in case of the sample with 0.1 equivalents and wanted to obtain a mixture of **8** and **Mes$_3$-Tr** in the case of the sample with 5 equivalents in order to be able to use the monoradical species **8** as an internal standard. The spectra in Fig. S8 are compared with the spectra that we assigned to **8** and **Mes$_3$-Tr**, respectively. The comparison clearly shows that the sample with 5 equivalents is a mixture of mono- and diradical species, as we had aimed for.

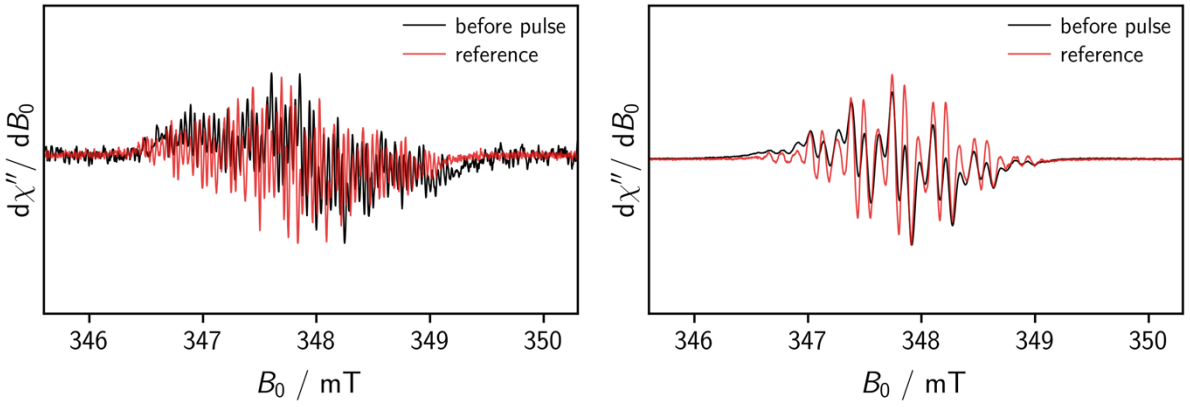

Fig. S8. Comparison of the room temperature cw EPR spectra of a 2.5 mM solution of **1a** + **1b** in toluene with 0.1 (left) and 5 equivalents (right) of the oxidant, recorded directly before the pulse EPR measurements, with the corresponding reference spectrum assigned to the monoradical **8** (left) and diradical **Mes$_3$-Tr** (right), respectively.

If the triplet state of **Mes$_3$-Tr** corresponds to the electronic ground state of the molecule, the EPR signal intensity is expected to increase when the temperature is lowered. To demonstrate this behavior, continuous wave EPR spectra were also recorded in frozen solution between 120 and 170 K. Fig. S9 shows the corresponding spectra recorded with a sample of a 1 mM solution of **1a** + **1b** with 5 equivalents of *p*-chloranil approximately 5 hours after oxidant addition. The microwave attenuation was set to 46 dB (0.0025 mW) and the modulation amplitude to 1 G. All experimental settings were kept the same between the measurements to assure that the relative signal intensities are comparable. From Fig. S8 it can clearly be seen that the signal intensity decreases with increasing temperature, strongly suggesting a triplet ground state. Likely due to the small expected *D* value, no half-field line could be detected for the diradical species **Mes$_3$-Tr** at temperatures of 100 K and above.

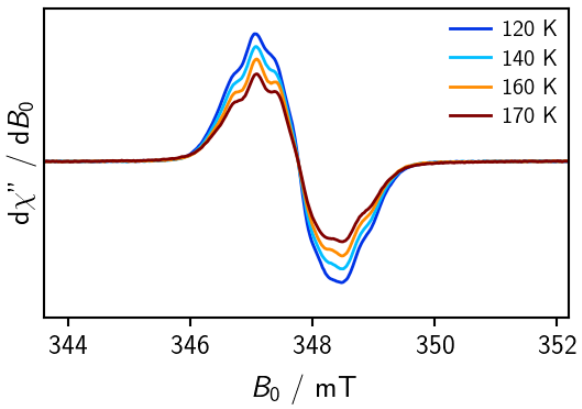

Fig. S9. Continuous wave EPR spectra of a 1 mM solution of **1a** + **1b** with 5 equivalents of the oxidant, recorded in frozen toluene solution at variable temperatures (as indicated) using a modulation amplitude of 1 G and a microwave attenuation of 46 dB.

To verify the persistence of the formed diradical species, room temperature X-band continuous wave EPR spectra were recorded after 3 hours, 2 weeks, and 3 weeks after oxidant addition and are shown in Fig. S10. The spectra were measured using the same experimental settings. The active part of the resonator was always completely filled (same active volume) and the Q-values of the cavity were very similar (4895, 5180, and 5062 for the spectra recorded after 3 hours, 2 weeks, and 3 weeks, respectively) so that the signal intensities are directly comparable. The diradical **Mes$_3$-Tr** was generated in the glove box by chemical oxidation of a 1 mM solution of the dihydro-precursor mixture (1a + 1b) in toluene using 5 equivalents of *p*-chloranil and transferred into an EPR tube which was subsequently sealed with Critoseal®. Between the EPR measurements, the sealed EPR tube was stored at room temperature.

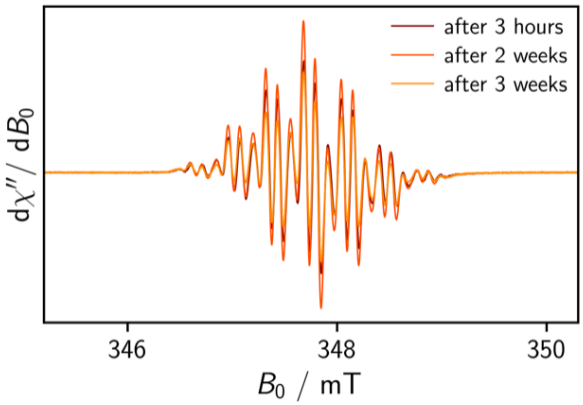

Fig. S10. Stability measurement of Mes_3-Tr. Room temperature X-band continuous wave EPR spectra were recorded after 3 hours, 2 weeks, and 3 weeks after oxidant addition. The spectra were measured using the same experimental settings so that the signal intensities are directly comparable.

Echo-detected field sweep

Echo-detected field-swept EPR spectra at the Q-band (34 GHz) were recorded using the sequence $\frac{\pi}{2} - \tau - \pi - \tau -$ echo with τ = 140 ns and a π-pulse length of 40 ns. Fig. S11 shows the spectra recorded for a 2.5 mM solution of **1a** + **1b** with either 0.1 or 5 equivalents of *p*-chloranil in frozen toluene solution at 120 K. The spectra were frequency corrected to 34.0 GHz and normalized for a comparison of the spectral shape.

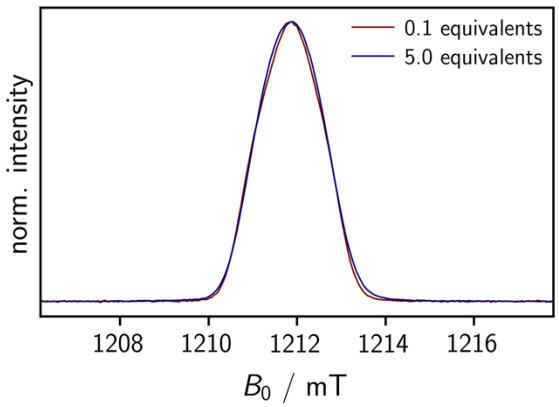

Fig. S11. Comparison of the echo-detected field-swept EPR spectra of frozen 2.5 mM solutions of **1a** + **1b** in toluene with 0.1 and 5 equivalents of the oxidant, recorded at 120 K.

Relaxation measurements

Spin coherence times (T_m) were measured using the pulse sequence $\frac{\pi}{2} - \tau - \pi - \tau -$ echo, where τ was gradually increased in steps of 16 or 4 ns, for the samples with 0.1 and 5 equivalents, respectively. A fit to the experimental data was performed assuming a mono-exponential decay of the form

$$I(\tau) = A \exp\left(-\frac{2\tau}{T_m}\right)$$

For the sample with 0.1 equivalents of the oxidant, a T_m value of 2.0 μs was measured, while for the sample with 5 equivalents a value of 0.6 μs was obtained at the position of the intensity maximum of the field-swept EPR spectrum (center of the spectrum).

The decay traces measured in frozen toluene at 120 K are shown in Fig. S12. As it would be expected for a diradical system with strong coupling between the unpaired spins, the phase memory time is considerably reduced in the sample with 5 equivalents of *p*-chloranil.

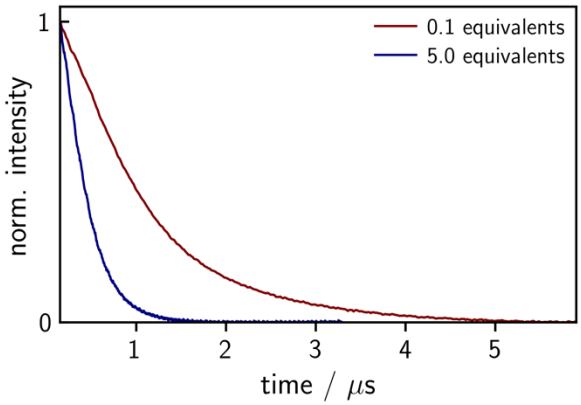

Fig. S12. Measurement of the spin coherence time (T_m) of frozen 2.5 mM solutions of **1a** + **1b** with 0.1 and 5 equivalents of the oxidant, recorded at 120 K at a magnetic field position corresponding to the intensity maximum (center) of the respective EPR spectra.

S6. DFT calculations

Calculations for the triangulene precursors **1**, the generated monoradicals **8** and triangulene were performed with the Gaussian 09 (Revision D.01)[17] suite of electronic structure programs. The geometries of the individual molecules were simplified by replacing the mesityl groups by hydrogen atoms. In addition, a pair of molecules with mesityl groups, **1a** and **1b**, were calculated to validate the effect of the peripheral substituents on the electronic transitions. The geometries were optimized at the B3LYP/6-31G(d) level of theory with the standard ultrafine integration grid. In the case of **1a** and **1b**, a finer integration grid (Superfine grid in Gaussian) was necessary to converge the optimization process to the local minimum. This grid was then used for all calculations of molecules with mesityl groups. The unrestricted formalism was used in calculations of open-shell molecules (doublet and triplet states). A frequency analysis was performed to confirm that the located stationary points represented local energy minima. Single point energies were computed with the B3LYP functional and cc-pVTZ basis set, the level of theory that successfully reproduced the experimental relative energies of **1a'** and **1b'** (for structures, see Supporting Tables 3 and 4) determined previously.[18] The reported final energies are at 0 K, that is, they represent the sum of the electronic energy and the zero-point vibrational energy correction. The latter was used unscaled. The electronic transitions were estimated with time-dependent DFT using B3LYP, PBE0 and BMK functionals and the 6-31G(d) basis set, considering 30 transitions to reduce the integration noise in the important low-energy excitations. Transitions with oscillator strengths $f > 0.01$ are reported unless stated otherwise. We found that the mesityl groups do not significantly affect either the energies or the oscillator strengths of individual electronic transitions in the triangular chromophores of **1**, **8** or triangulene.

Table S3. TD-DFT-calculated relative energies, absorption maxima and corresponding oscillator strengths (only $f > 0.01$ are shown) for 1a′

Dihydro-precursor 1a′

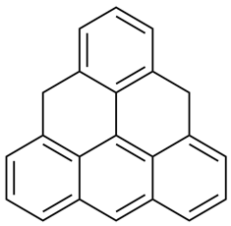

Relative energy = 1.3 kcal mol^{-1}

B3LYP

	Energy / eV	Wavelength / nm	Oscillator strength *f*
S_1	**2.7668**	**448.11**	**0.1753**
S_5	4.1369	299.70	0.0174
S_7	4.3912	282.35	0.0573
S_9	4.8780	254.17	0.8244

BMK

	Energy / eV	Wavelength / nm	Oscillator strength *f*
S_1	**3.0230**	**410.14**	**0.2155**
S_4	4.4826	276.59	0.0175
S_5	4.6325	267.64	0.0829
S_6	4.8843	253.84	0.0447
S_8	4.9955	248.19	0.1241

PBE0

	Energy / eV	Wavelength / nm	Oscillator strength *f*
S_1	**2.8376**	**436.93**	**0.1856**
S_5	4.2802	289.67	0.0275
S_7	4.5293	273.74	0.0553
S_8	4.7055	263.49	0.0158
S_9	4.9917	248.38	0.8715

Table S4. TD-DFT-calculated relative energies, absorption maxima and corresponding oscillator strengths (only $f > 0.01$ are shown) for 1b′

Dihydro-precursor 1b′

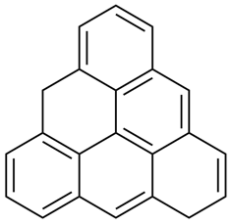

Relative energy = 0.0 kcal mol^{-1}

B3LYP

	Energy / eV	Wavelength / nm	Oscillator strength *f*
S_3	**3.7886**	**327.25**	**0.1625**
S_4	**4.0305**	**307.61**	**0.4806**
S_5	4.3379	285.81	0.0126
S_6	4.4823	276.61	0.0101
S_7	4.6456	266.88	0.0188
S_9	4.8616	255.03	0.0569

BMK

	Energy / eV	Wavelength / nm	Oscillator strength *f*
S_3	**4.2764**	**289.93**	**0.2946**
S_4	**4.3935**	**282.20**	**0.5904**
S_5	4.6958	264.03	0.0117
S_6	5.0110	247.42	0.0160

PBE0

	Energy /eV	Wavelength / nm	Oscillator strength *f*
S_3	**3.9211**	**316.20**	**0.1873**
S_4	**4.1323**	**300.03**	**0.5135**
S_5	4.4428	279.07	0.0136
S_6	4.6229	268.19	0.0115
S_7	4.8059	257.98	0.0204
S_9	5.0075	247.60	0.0489

Table S5. TD-DFT-calculated relative energies, absorption maxima and corresponding oscillator strengths (only $f > 0.01$ are shown) for 1a

Dihydro-precursor 1a

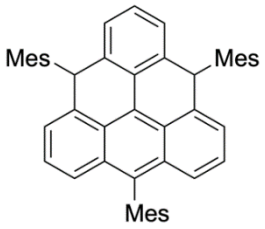

Relative energy (*syn*) = 6.6 kcal mol^{-1} Relative energy (*anti*)= 6.5 kcal mol^{-1}

B3LYP *syn*-1a

	Energy / eV	Wavelength / nm	Oscillator strength *f*
S_1	**2.6997**	**459.26**	**0.2625**
S_{15}	4.3625	284.20	0.0347
S_{17}	4.4533	278.41	0.0347
S_{18}	4.4940	275.89	0.0610
S_{19}	4.5353	273.38	0.0226
S_{20}	4.6049	269.25	0.0110
S_{21}	4.7832	259.21	0.7509

B3LYP *anti*-1a

	Energy / eV	Wavelength / nm	Oscillator strength *f*
S_1	**2.7060**	**458.19**	**0.2633**
S_4	3.7731	328.60	0.0133
S_{15}	4.3554	284.67	0.0143
S_{16}	4.3855	282.72	0.0291
S_{17}	4.4583	278.10	0.0457
S_{18}	4.4821	276.62	0.0512
S_{19}	4.5471	272.67	0.0224
S_{20}	4.5914	270.03	0.0112
S_{21}	4.7841	259.16	0.7520

Table S6. TD-DFT-calculated relative energies, absorption maxima and corresponding oscillator strengths (only $f > 0.01$ are shown) for 1b

Dihydro-precursor 1b

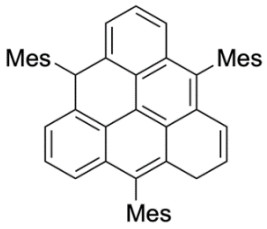

Relative energy = 0.0 kcal mol^{-1}

B3LYP

	Energy / eV	Wavelength / nm	Oscillator strength *f*
S_2	3.5530	348.95	0.0159
S_3	**3.7421**	**331.33**	**0.2310**
S_4	**3.9447**	**314.31**	**0.6022**
S_6	4.2893	289.06	0.0248
S_7	4.3203	286.98	0.0127
S_{11}	4.5093	274.95	0.0186
S_{12}	4.5193	274.34	0.0135
S_{25}	4.8379	256.28	0.0535
S_{27}	4.8864	253.73	0.0154
S_{30}	4.9563	250.15	0.0324

Table S7. TD-DFT-calculated relative energies, absorption maxima and corresponding oscillator strengths (only $f > 0.01$ are shown) for 8a′

Monoradical 8a′

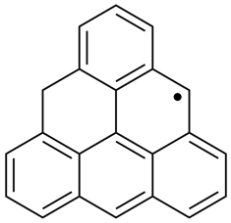

Relative energy (**8a′**) = –2.3 kcal mol^{-1}
Relative energy (**8a**) = –3.4 kcal mol^{-1}

B3LYP

	Energy / eV	Wavelength / nm	Oscillator strength *f*
S_2	**2.4652**	**502.93**	**0.0566**
S_7	3.2076	386.54	0.0484
S_8	3.3752	367.34	0.0900
S_{10}	3.6383	340.77	0.1001
S_{12}	3.9346	315.11	0.3539
S_{15}	4.2365	292.66	0.0108
S_{22}	4.6804	264.90	0.0161
S_{26}	4.8537	255.44	0.2241

BMK

	Energy / eV	Wavelength / nm	Oscillator strength *f*
S_3	**2.7794**	**446.09**	**0.0716**
S_6	3.4860	355.67	0.0675
S_8	3.6531	339.40	0.2046
S_{10}	4.0335	307.38	0.0724
S_{12}	4.3015	288.23	0.4292
S_{15}	4.6524	266.49	0.0179

PBE0

	Energy / eV	Wavelength / nm	Oscillator strength *f*
S_3	**2.6306**	**471.31**	**0.0603**
S_7	3.3539	369.67	0.0474
S_9	3.5340	350.83	0.1219
S_{11}	3.8186	324.68	0.0714
S_{12}	4.0497	306.16	0.3815
S_{23}	4.8390	256.22	0.0220

Table S8. TD-DFT-calculated relative energies, absorption maxima and corresponding oscillator strengths (only $f > 0.01$ are shown) for 8b′

Monoradical 8b′

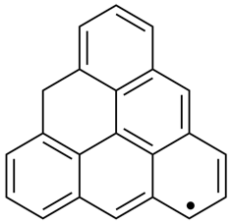

Relative energy (**8b′**) = 0.0 kcal mol^{-1}
Relative energy (**8b**) = 0.0 kcal mol^{-1}

B3LYP

	Energy / eV	Wavelength / nm	Oscillator strength *f*
S_2	**2.4132**	**513.77**	**0.1377**
S_6	3.2157	385.55	0.0430
S_7	3.3861	366.15	0.0222
S_9	3.4685	357.46	0.0196
S_{10}	3.6547	339.24	0.0305
S_{11}	3.7784	328.14	0.0712
S_{19}	4.3762	283.31	0.0220
S_{26}	4.8973	253.17	0.1184

BMK

	Energy / eV	Wavelength / nm	Oscillator strength *f*
S_2	**2.4132**	**513.77**	**0.1377**
S_6	3.2157	385.55	0.0430
S_7	3.3861	366.15	0.0222
S_9	3.4685	357.46	0.0196
S_{10}	3.6547	339.24	0.0305
S_{19}	4.8579	255.22	0.0133

PBE0

	Energy / eV	Wavelength / nm	Oscillator strength *f*
S_2	**2.4132**	**513.77**	**0.1377**
S_6	3.2157	385.55	0.0430
S_7	3.3861	366.15	0.0222
S_9	3.4685	357.46	0.0196
S_{10}	3.6547	339.24	0.0305
S_{11}	3.7784	328.14	0.0712
S_{19}	4.3762	283.31	0.0220
S_{23}	4.8517	255.55	0.0694

Table S9. TD-DFT-calculated relative energies, absorption maxima and corresponding oscillator strengths (only $f > 0.01$ are shown) for triangulene

Triangulene			
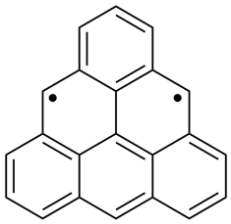			
B3LYP			
	Energy / eV	Wavelength / nm	Oscillator strength f
S_1	2.6461	468.56	0.0004
S_2	2.6472	468.35	0.0004
S_3	2.9103	426.02	0.0018
S_4	2.9111	425.91	0.0018
S_8	3.2289	383.98	0.0184
S_9	3.2290	383.97	0.0186
S_{10}	3.2908	376.76	0.0082
S_{11}	3.2920	376.62	0.0082
S_{12}	3.4227	362.24	0.0122
S_{13}	3.4235	362.15	0.0126
S_{15}	**3.9160**	**316.61**	**0.4307**
S_{16}	**3.9162**	**316.60**	**0.4308**
BMK			
	Energy / eV	Wavelength / nm	Oscillator strength f
S_1	2.8626	433.12	0.0004
S_2	2.8643	432.87	0.0004
S_3	3.1045	399.37	0.0020
S_4	3.1053	399.27	0.0020
S_7	3.5433	349.91	0.0321
S_8	3.5437	349.88	0.0319
S_{10}	3.7185	333.43	0.0203
S_{11}	3.7200	333.29	0.0208
S_{12}	3.8195	324.61	0.0466
S_{13}	3.8197	324.59	0.0476
S_{14}	**4.2291**	**293.17**	**0.5181**
S_{15}	**4.2300**	**293.11**	**0.5173**

PBE0			
	Energy / eV	Wavelength / nm	Oscillator strength *f*
S_1	2.7851	445.17	0.0005
S_2	2.7864	444.97	0.0005
S_3	3.0307	409.09	0.0019
S_4	3.0314	409.00	0.0020
S_8	3.4070	363.91	0.0237
S_9	3.4071	363.90	0.0235
S_{10}	3.5050	353.74	0.0110
S_{11}	3.5063	353.60	0.0111
S_{12}	3.6317	341.40	0.0156
S_{13}	3.6323	341.34	0.0161
S_{15}	**4.0819**	**303.74**	**0.4530**
S_{16}	**4.0822**	**303.72**	**0.4530**
S_{21}	4.8597	255.13	0.0011
S_{22}	4.8614	255.04	0.0012

DFT calculations of hyperfine coupling constants and spin densities

Calculations for the generated monoradicals **8** and the triplet diradical **Mes$_3$-Tr** were performed using the ORCA program package (Version 4.0).[19] For the calculation of the spin densities, the structures were first optimized in their doublet or triplet ground states using the B3LYP functional in combination with the def2-TZVP basis set. The RI approximation was employed (RIJCOSX) using the def2/J auxiliary basis set. Magnetic property calculations in the doublet or triplet states used the B3LYP functional in combination with the EPR-II basis set.

DFT predicts near identical *g* values for all three structures of 2.0026. A visual representation of the optimized molecular structures and calculated spin densities (iso value of 0.001) is shown in Fig. S13. Fig. S14 shows a visual representation of the calculated anisotropic proton hyperfine coupling tensors for the three structures and gives an overview over the corresponding isotropic values which were used in the simulations. A summary of the isotropic values is provided in Table S10. All hyperfine couplings smaller than 0.5 MHz were neglected here since they are not resolved in the experimental spectra and only contribute to the linewidth.

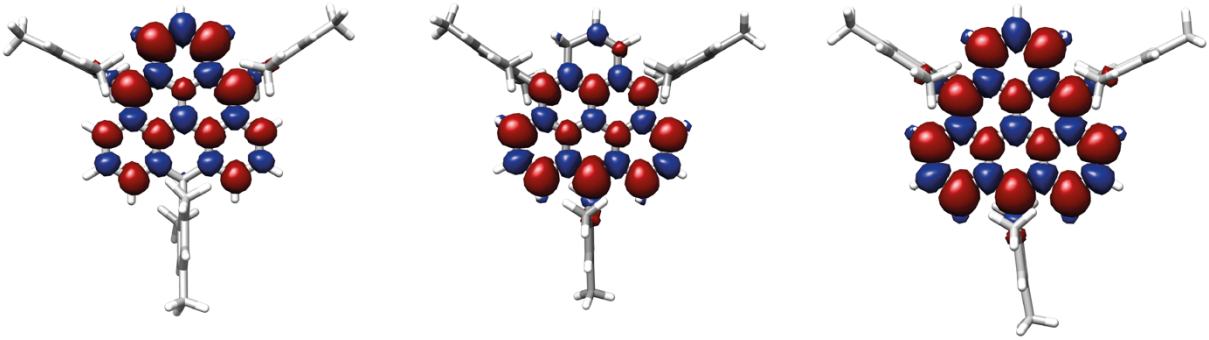

Fig. S13. Visualization of the spin density in the doublet state of **8a** and **8b** (left and center, respectively) and in the triplet state of **Mes$_3$-Tr** (right) as predicted by DFT calculations.

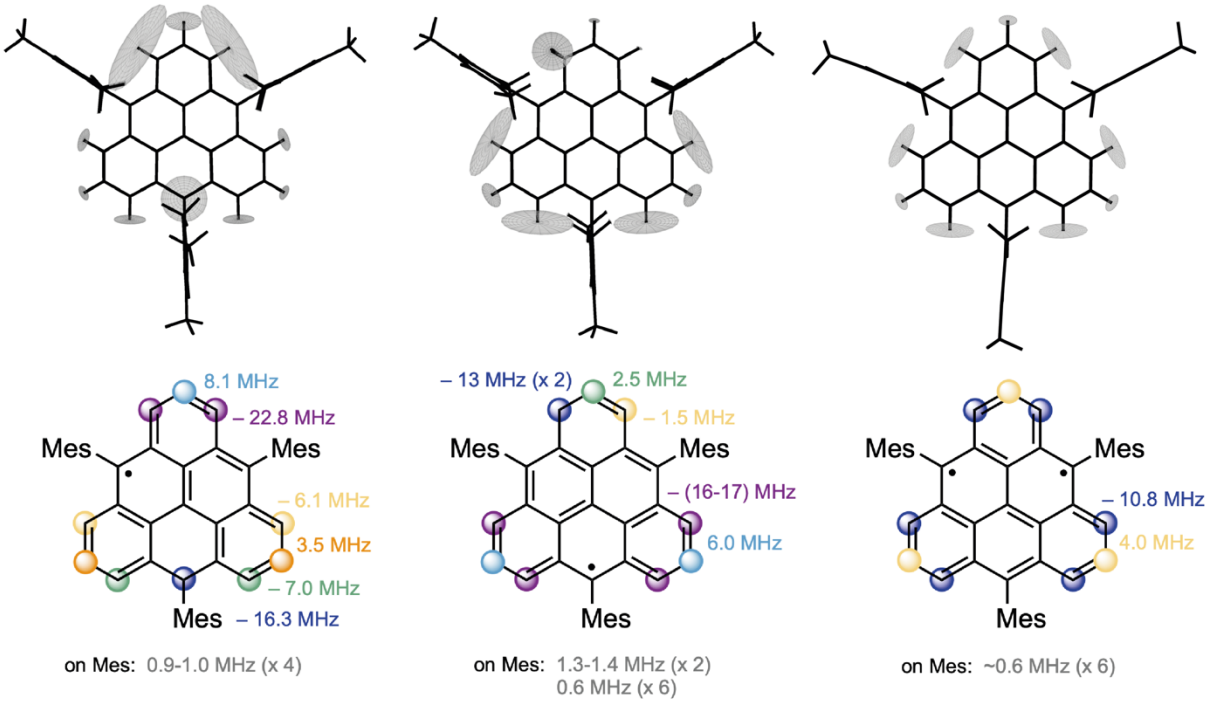

Fig. S14. Visualization of the calculated proton hyperfine coupling tensors associated with the doublet state of **8a** and **8b** (left and center, respectively) and the triplet state of **Mes$_3$-Tr** (right). The tensors are placed at the position of the individual protons and have been scaled by the same value in all cases for illustration purposes. The illustration below shows the corresponding isotropic hyperfine coupling constants as needed for the simulations of the room temperature cw EPR spectra. Similar values have been grouped and only calculated hyperfine coupling constants larger than 0.5 MHz are considered. All smaller couplings are assumed to contribute to the linewidth only.

Table S10. Overview of the calculated isotropic ^{1}H hyperfine coupling constants for 8a, 8b and Mes$_3$-Tr as used in the simulations

Set	Monoradical **8a**	Monoradical **8b**	Diradical **Mes$_3$-Tr**
1	−22.9 MHz (× 1)	−17.4 MHz (× 1)	−10.9 MHz (× 1)
2	−22.7 MHz (× 1)	−17.1 MHz (× 1)	−10.8 MHz (× 4)
3	−16.4 MHz (× 1)	−16.0 MHz (× 1)	−10.7 MHz (× 1)
4	8.1 MHz (× 1)	−15.6 MHz (× 1)	4.0 MHz (× 3)
5	−7.0 MHz (× 1)	−13.7 MHz (× 1)	0.6 MHz (× 6)
6	−6.9 MHz (× 1)	−12.6 MHz (× 1)	–
7	−6.2 MHz (× 1)	6.1 MHz (× 1)	–
8	−6.1 MHz (× 1)	5.7 MHz (× 1)	–
9	3.5 MHz (× 2)	2.5 MHz (× 1)	–
10	1.0 MHz (× 1)	−1.5 MHz (× 1)	–
11	0.97 MHz (× 1)	1.4 MHz (× 1)	–
12	0.96 MHz (× 1)	1.3 MHz (× 1)	–
13	0.95 MHz (× 1)	0.66 MHz (× 3)	–
14	–	0.60 MHz (× 3)	–

Near identical values were grouped to form sets of equivalent protons and only couplings larger than 0.5 MHz were considered. The couplings of the methyl group protons on the mesityl side groups were averaged since the methyl group is assumed to be freely rotating. The number of equivalent protons is given in parentheses and the couplings of protons on the mesityl side groups are marked in gray. In the simulations of the spectra, shown in Fig. 3, a scaling factor of 0.93 was applied to all proton couplings listed above.

Calculation of the singlet–triplet energy gap for Mes$_3$-Tr

The exchange coupling parameter J was calculated by comparing the energies of triplet and broken-symmetry (singlet) wavefunctions, using the Yamaguchi formalism[20,21]

$$J = \frac{E_{\mathrm{BS}} - E_{\mathrm{T}}}{\langle S^2 \rangle_{\mathrm{T}} - \langle S^2 \rangle_{\mathrm{BS}}}$$

where E_{BS} is the energy of the broken-symmetry (singlet) state, E_{T} is the energy of the triplet state, and $\langle S^2 \rangle_{\mathrm{BS}}$ and $\langle S^2 \rangle_{\mathrm{T}}$ are the expectation values of S^2 for the broken symmetry and triplet states. The SCF convergence criteria were set to 10^{-8} (default) and 10^{-12} for the geometry optimizations and single-point calculations, respectively.

From an initial converged triplet geometry and wavefunction, a broken symmetry guess at the triplet geometry was converged to generate the singlet solution. This yielded a J value of 2235 cm^{-1}.

Since the DFT calculations make use of the following Hamiltonian

$$\widehat{\mathcal{H}}_{\mathrm{J}} = -2J\,\hat{S}_1\hat{S}_2$$

a positive J value indicates ferromagnetic coupling ($E_{\mathrm{T}} < E_{\mathrm{S}}$), in agreement with the experimental observations. From this calculation, the singlet–triplet gap ($2J$) is thus estimated to be about 12.8 $\mathrm{kcal\,mol}^{-1}$.

Using the same procedure for the parent triangulene molecule without the three mesityl side groups, a value of 13.2 $\mathrm{kcal\,mol}^{-1}$ is obtained, which is in good agreement with previous literature results.[22]

S7. Copies of NMR and HRMS spectra

^{1}H NMR / 400 MHz / $CDCl_3$

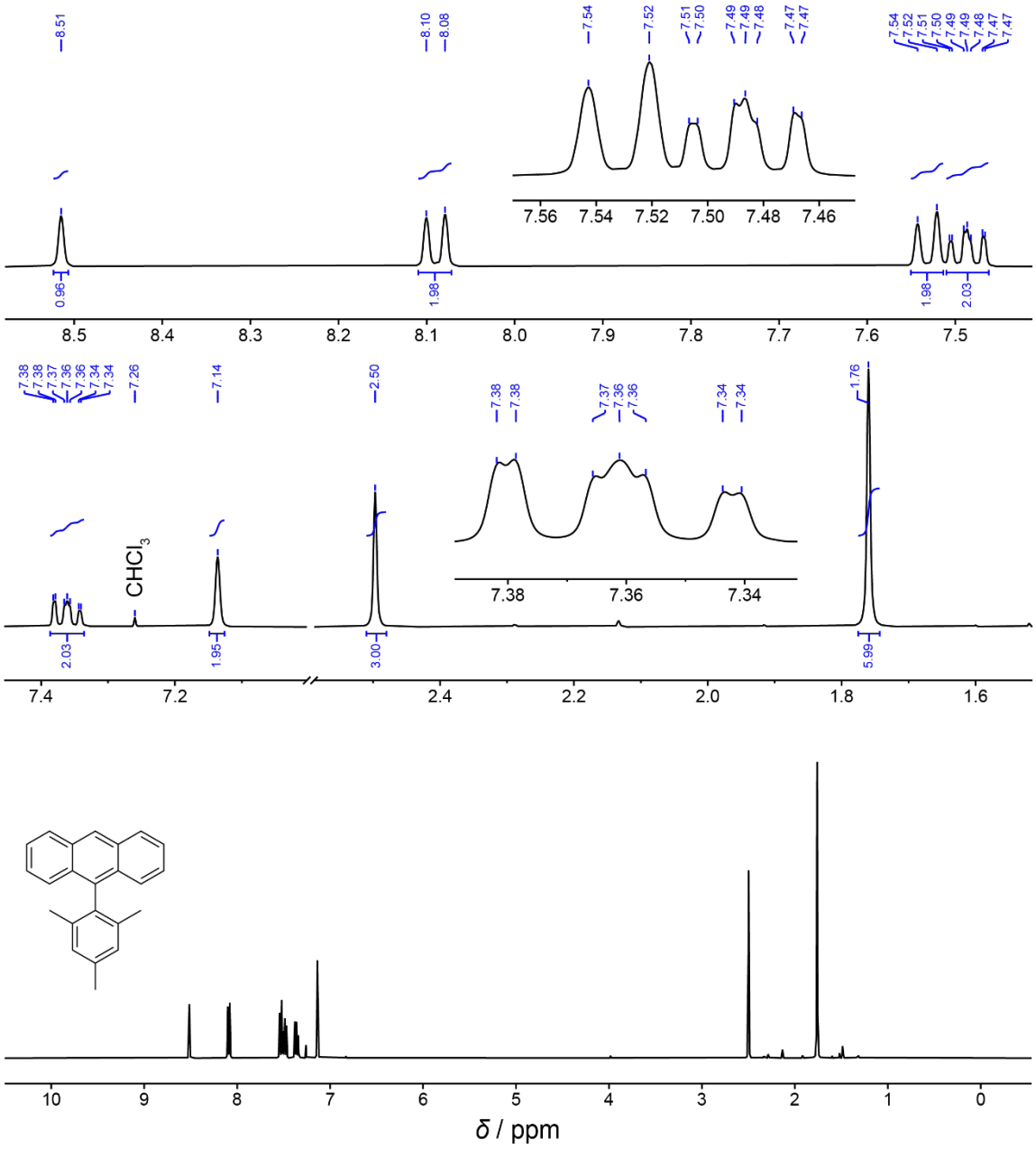

^{13}C NMR / 101 MHz / $CDCl_3$

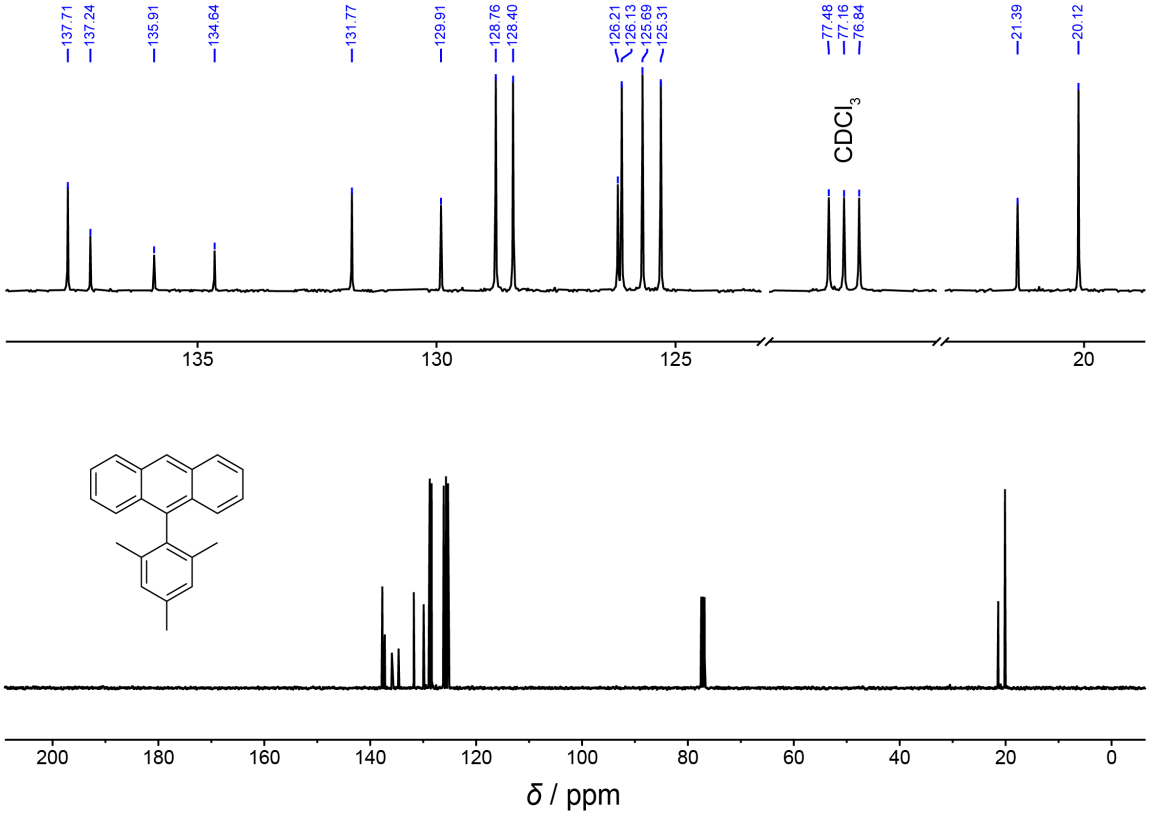

^{1}H NMR / 400 MHz / $CDCl_3$

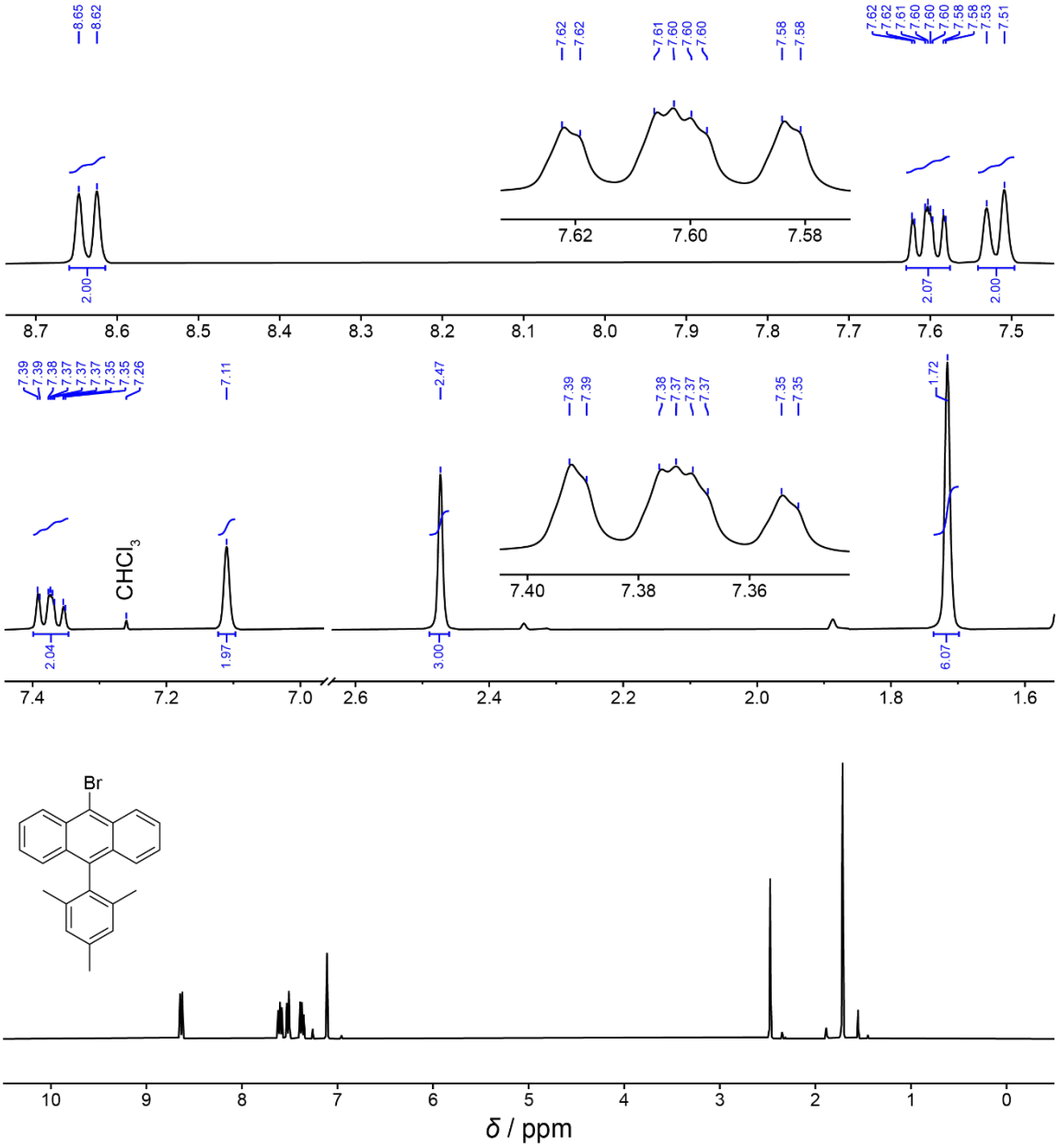

^{13}C NMR / 101 MHz / $CDCl_3$

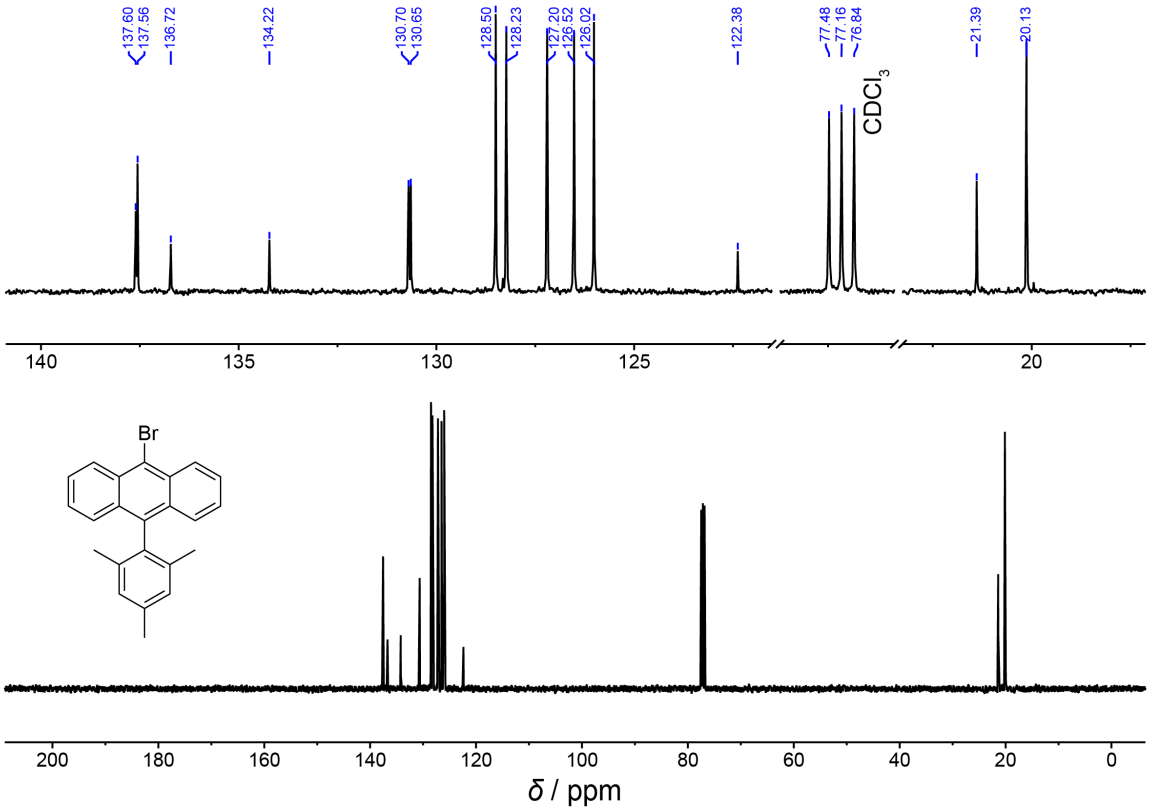

^{1}H NMR / 500 MHz / $CDCl_3$

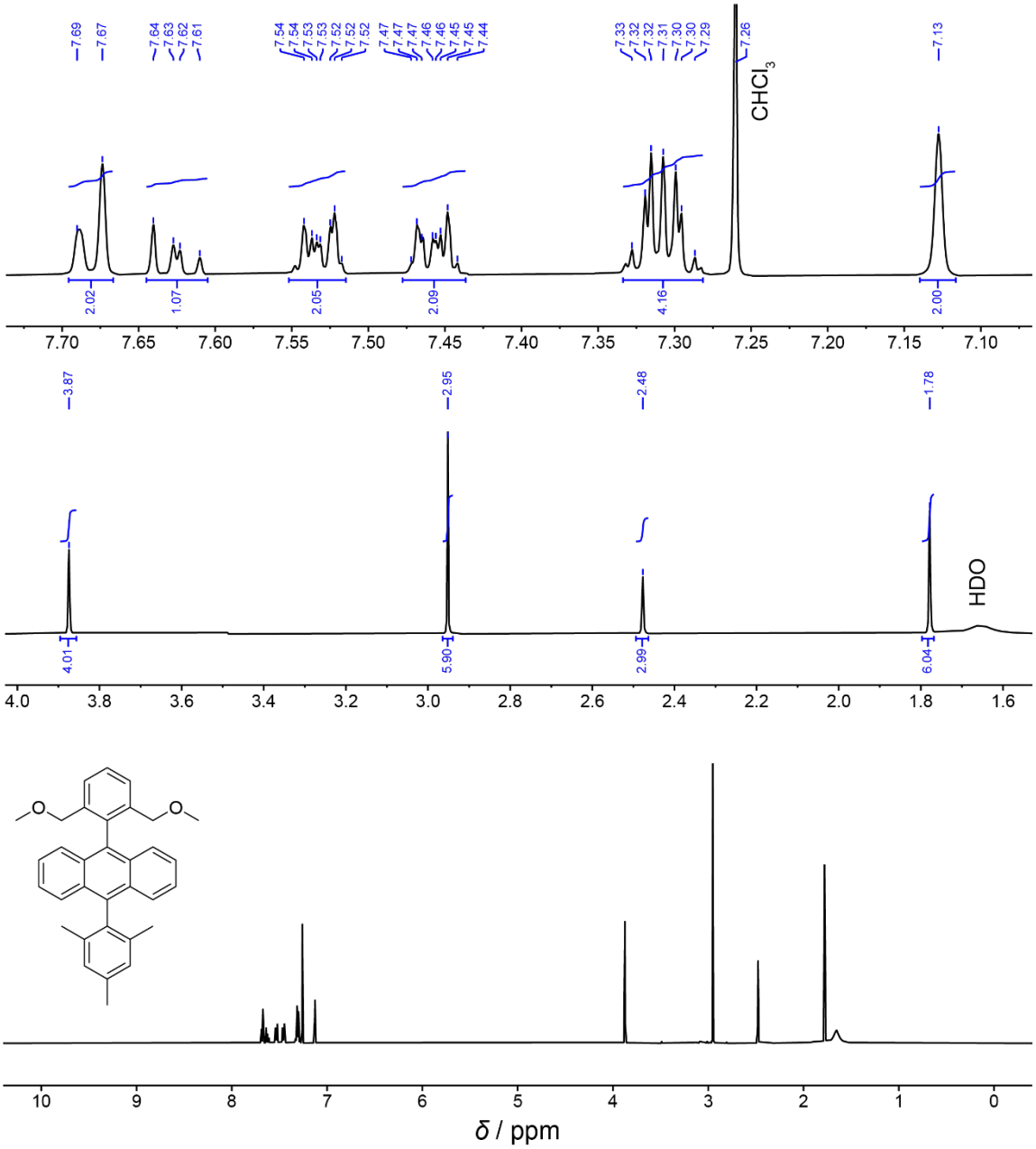

^{13}C NMR / 126 MHz / $CDCl_3$

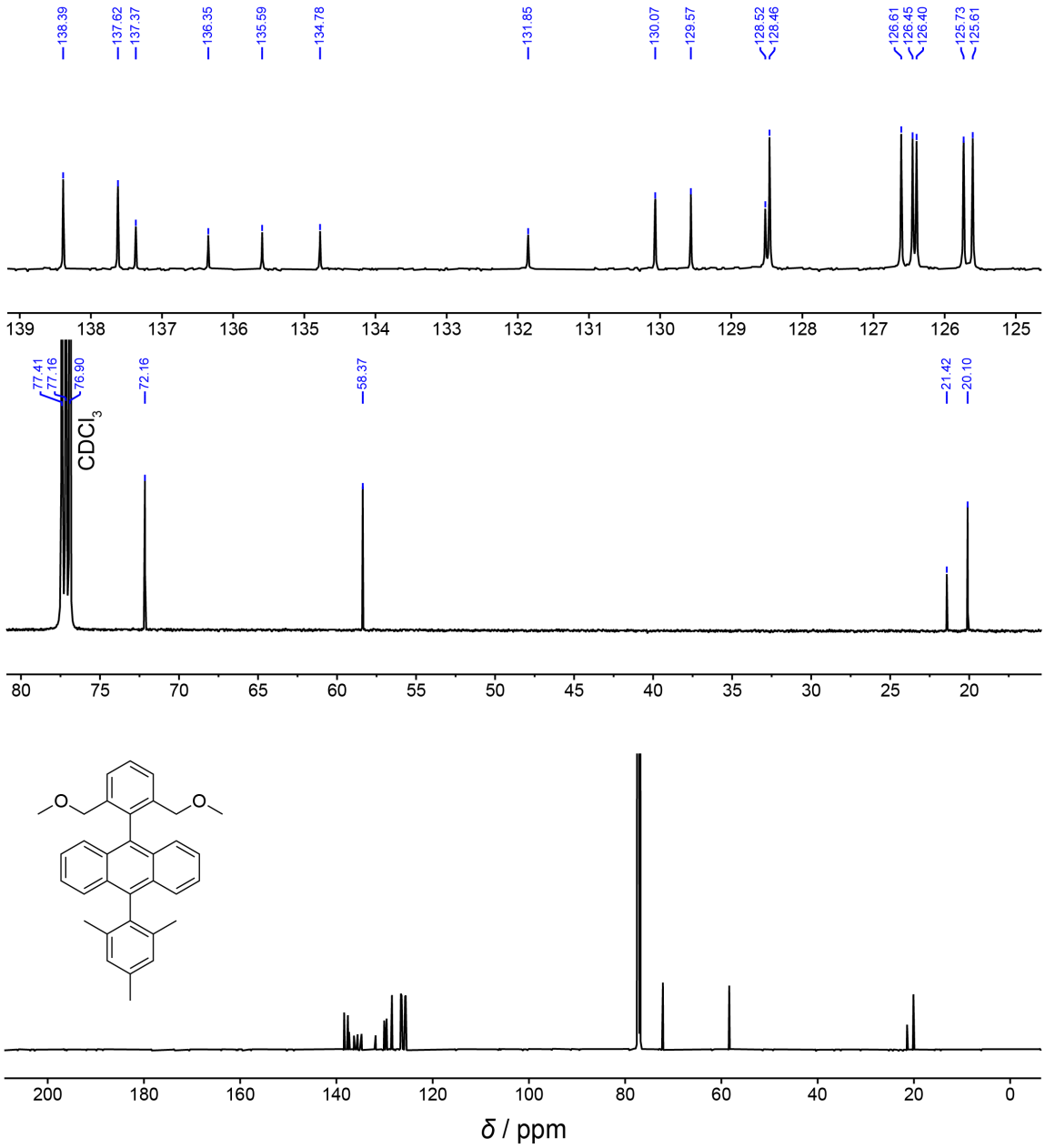

D:\Data\Service\Data\20_juQEx_1527 11/02/20 11:59:13 Sample: LV_417

Client: (+)-HR-ESI-MS Solvent: MeOH/CHCl3 3:2

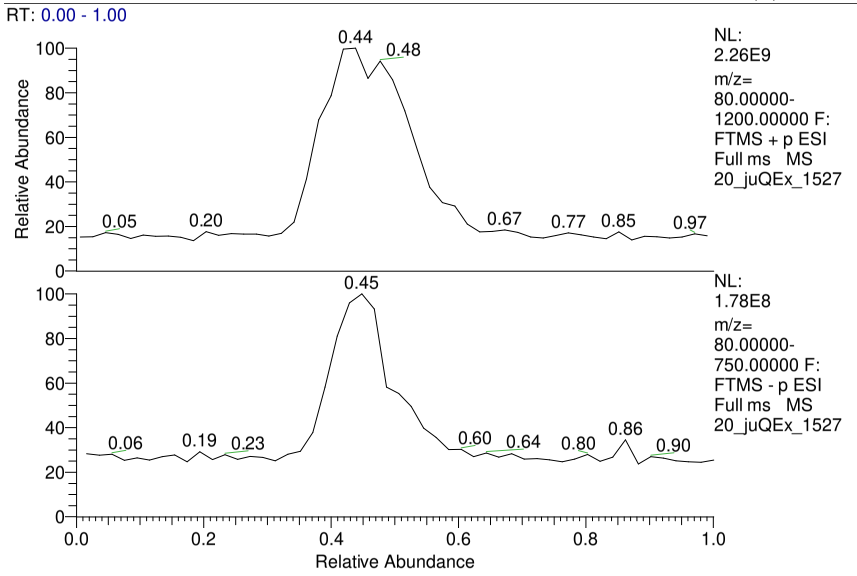

20_juQEx_1527#41-47 RT: 0.40-0.46 AV: 4
SB: 25 0.04-0.24 , 0.71-0.97
T: FTMS + p ESI Full lock ms [100.0000-1500.0000]
m/z= 482.67816-484.04678

m/z	Intensity	Relative	Theo. Mass	Delta (ppm)	RDB equiv.	Composition
483.22931	189361728.0	100.00	483.22917	0.28	21.5	$C_{31}H_{27}N_6$
			483.22945	-0.30	17.5	$C_{33}H_{32}O_2Na$
			483.22968	-0.78	3.5	$C_{18}H_{35}O_{11}N_4$
			483.22996	-1.35	5.0	$C_{19}H_{34}O_8N_5Na$
			483.22862	1.41	0.0	$C_{18}H_{38}O_{12}NNa$
			483.22862	1.43	5.5	$C_{17}H_{32}O_7N_8Na$
			483.22834	1.99	4.0	$C_{16}H_{33}O_{10}N_7$
			483.22811	2.48	18.0	$C_{31}H_{30}ON_3Na$
			483.23051	-2.50	21.0	$C_{33}H_{29}ON_3$
			483.22783	3.04	16.5	$C_{30}H_{31}O_4N_2$
			483.23102	-3.55	8.5	$C_{19}H_{31}O_7N_8$
			483.23103	-3.56	3.0	$C_{20}H_{37}O_{12}N$
			483.23130	-4.13	4.5	$C_{21}H_{36}O_9N_2Na$
			483.22728	4.19	0.5	$C_{16}H_{36}O_{11}N_4Na$

20_juQEx_1527 #40-47 RT: 0.40-0.46 AV: 4 SB: 24 0.03-0.23 , 0.70-0.95 NL: 5.46E8
T: FTMS + p ESI Full lock ms [100.0000-1500.0000]

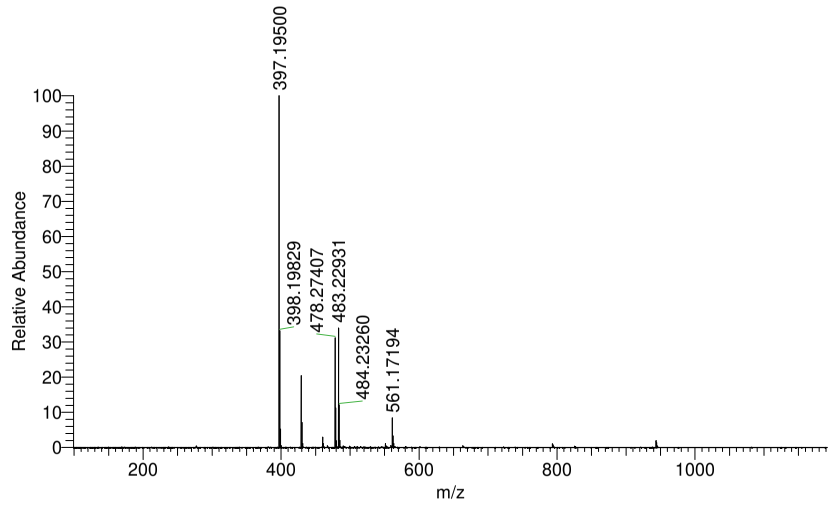

20_juQEx_1527 #40-46 RT: 0.40-0.44 AV: 3 SB: 25 0.03-0.24 , 0.70-0.95 NL: 1.83E8
T: FTMS + p ESI Full lock ms [100.0000-1500.0000]

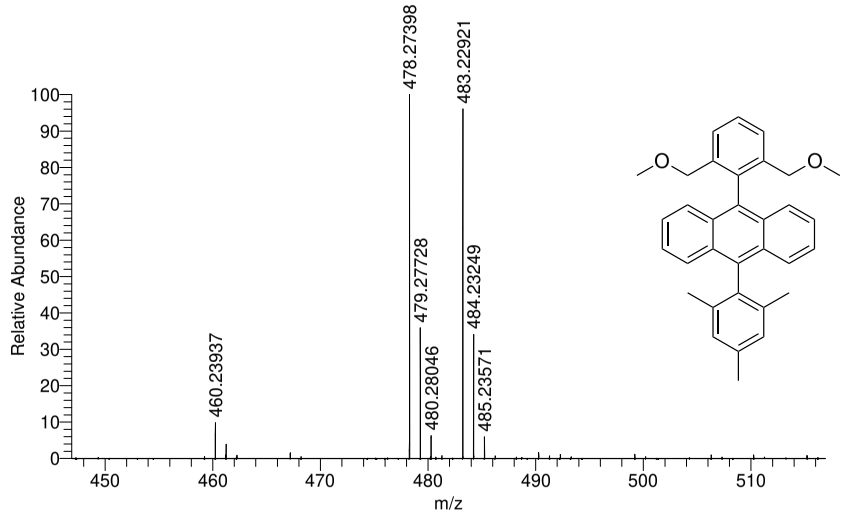

^{1}H NMR / 400 MHz / $CDCl_3$

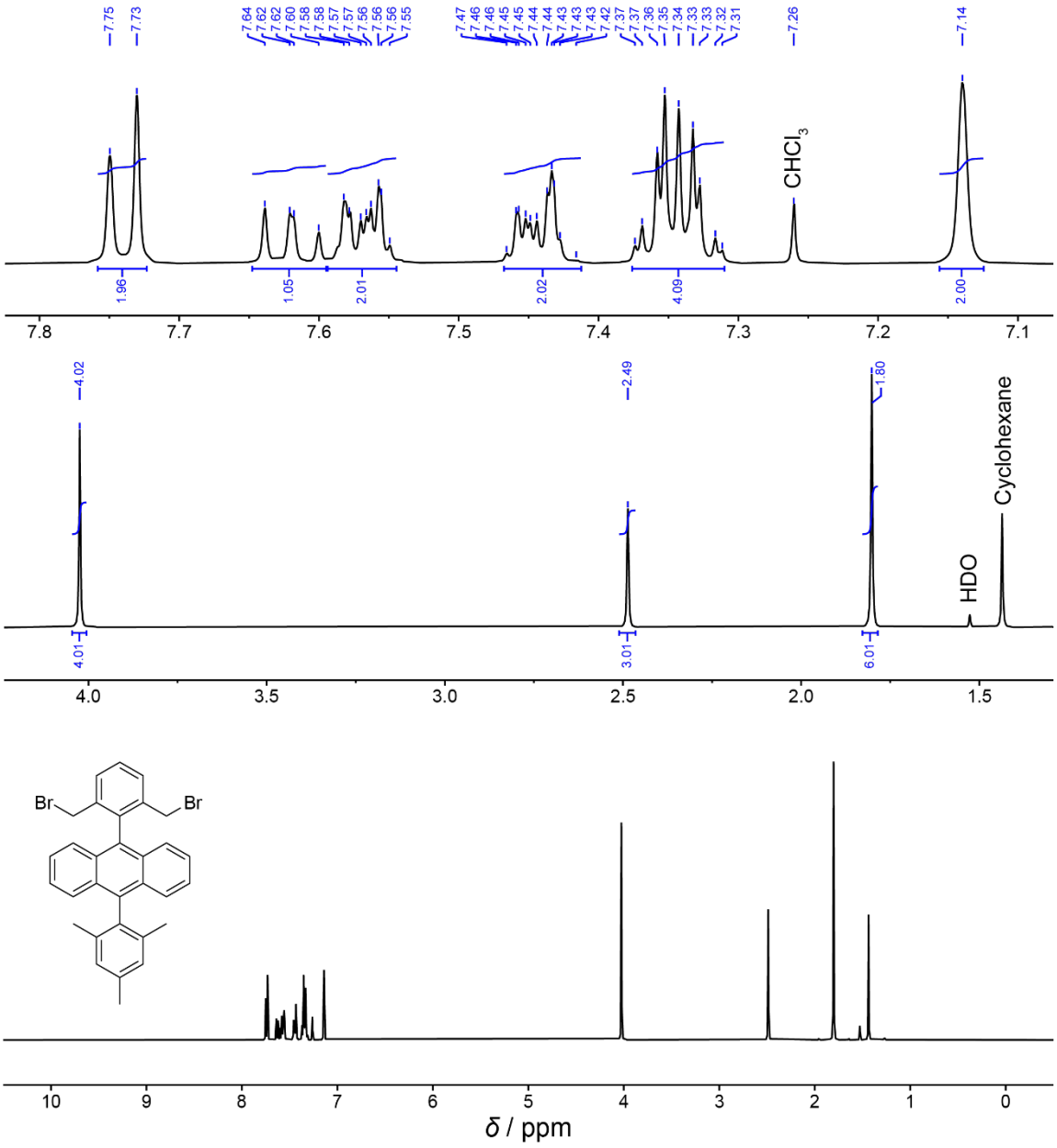

^{13}C NMR / 101 MHz / $CDCl_3$

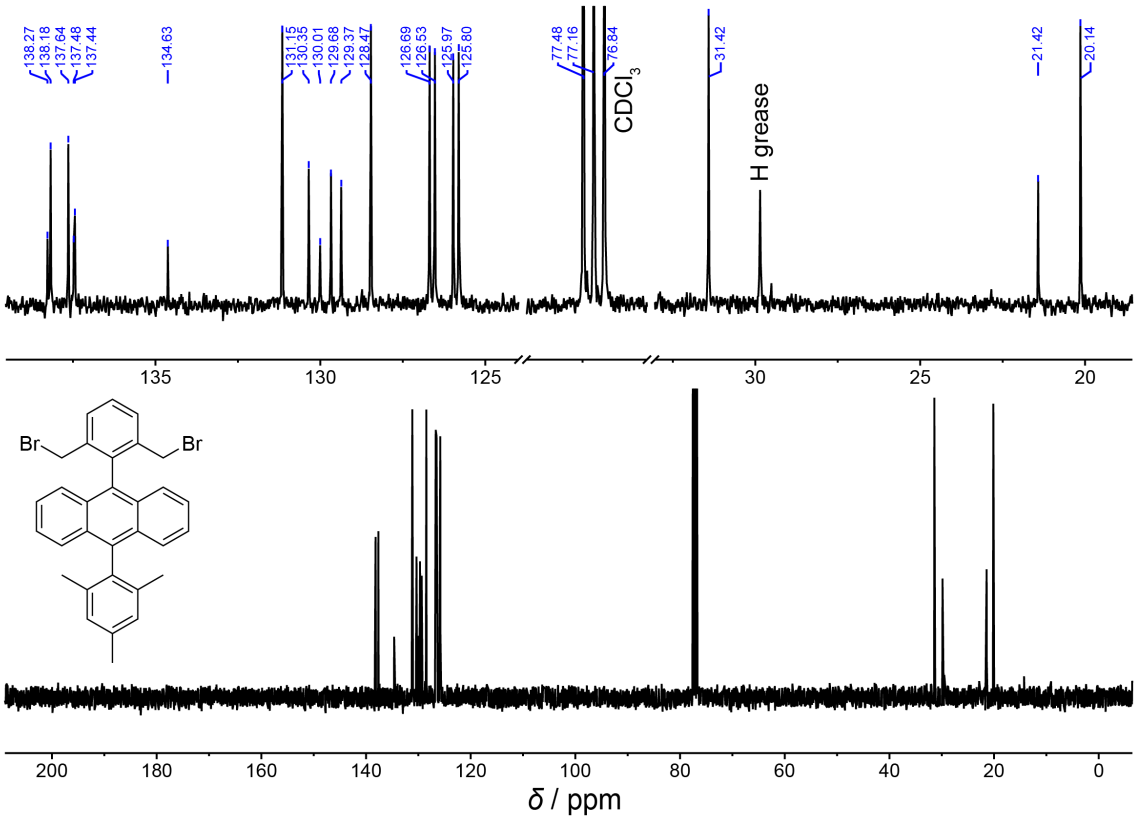

HR-EI-Report (Thermo DFS)

Sample: Client:

6340cohr-cmass2 #14-20 RT: 0.98-1.43 AV: 7 NL: 1.32E6
T: + c EI Full ms [527.56-583.56]

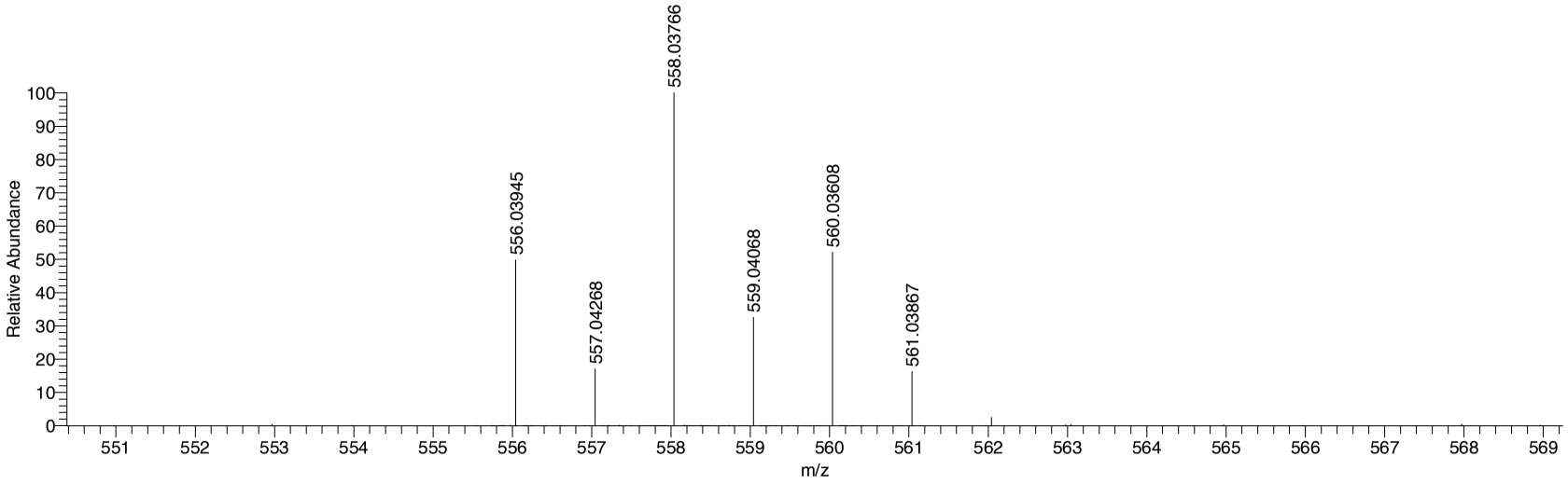

6340cohr-cmass2#14-20 RT: 0.98-1.43 AV: 7
T: + c EI Full ms [527.56-583.56]
m/z= 555.76127-556.28159

m/z	Intensity	Relative	Theo. Mass	Delta (ppm)	Composition
556.03945	655784.0	100.00	556.03958	-0.24	$C_{31}H_{26}Br_2$
			556.03930	0.25	$C_{42}H_6O_2N$

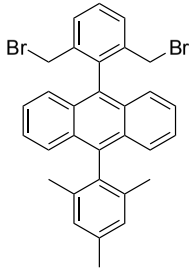

^{1}H NMR / 400 MHz / $CDCl_3$

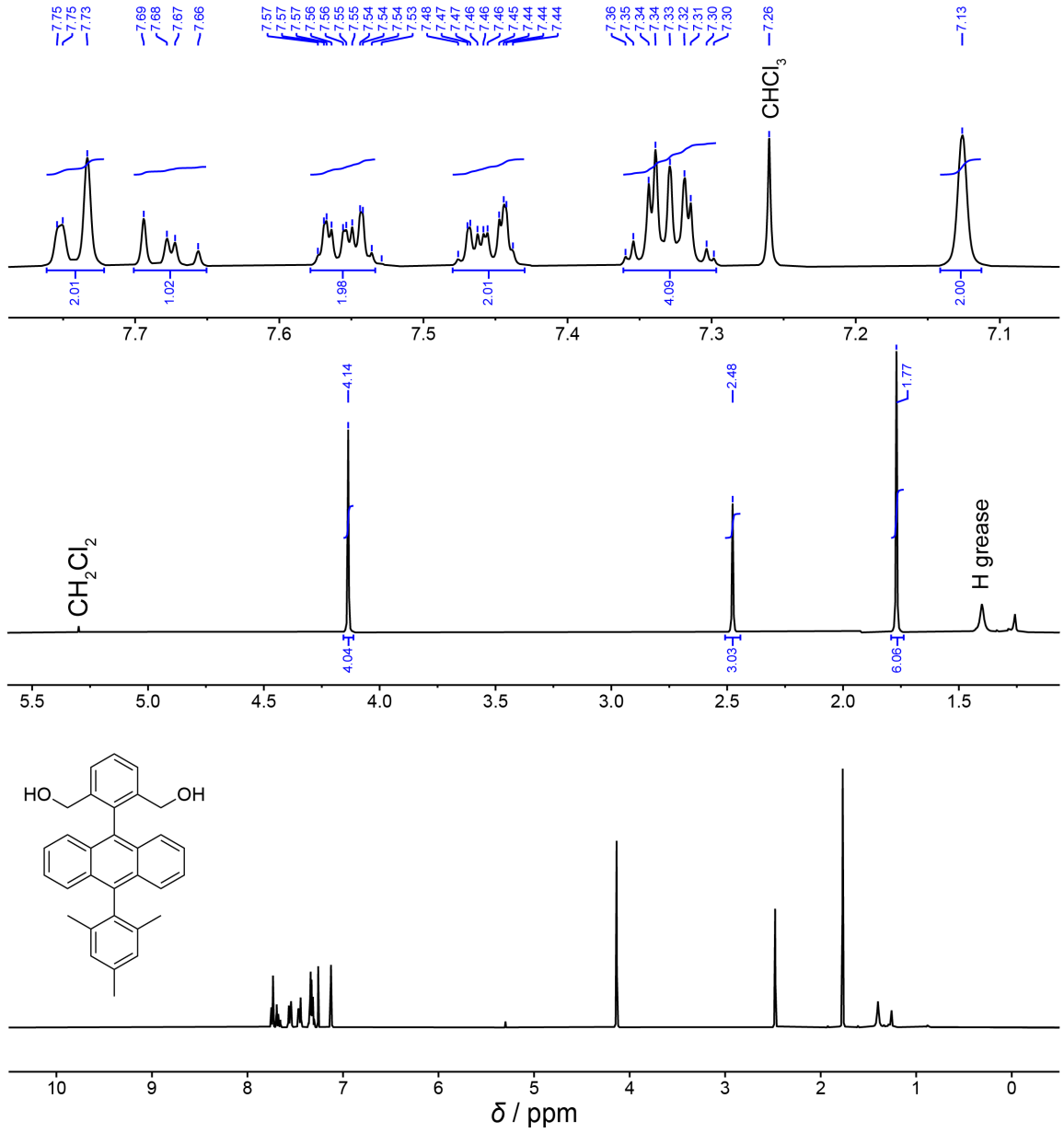

^{13}C NMR / 101 MHz / $CDCl_3$

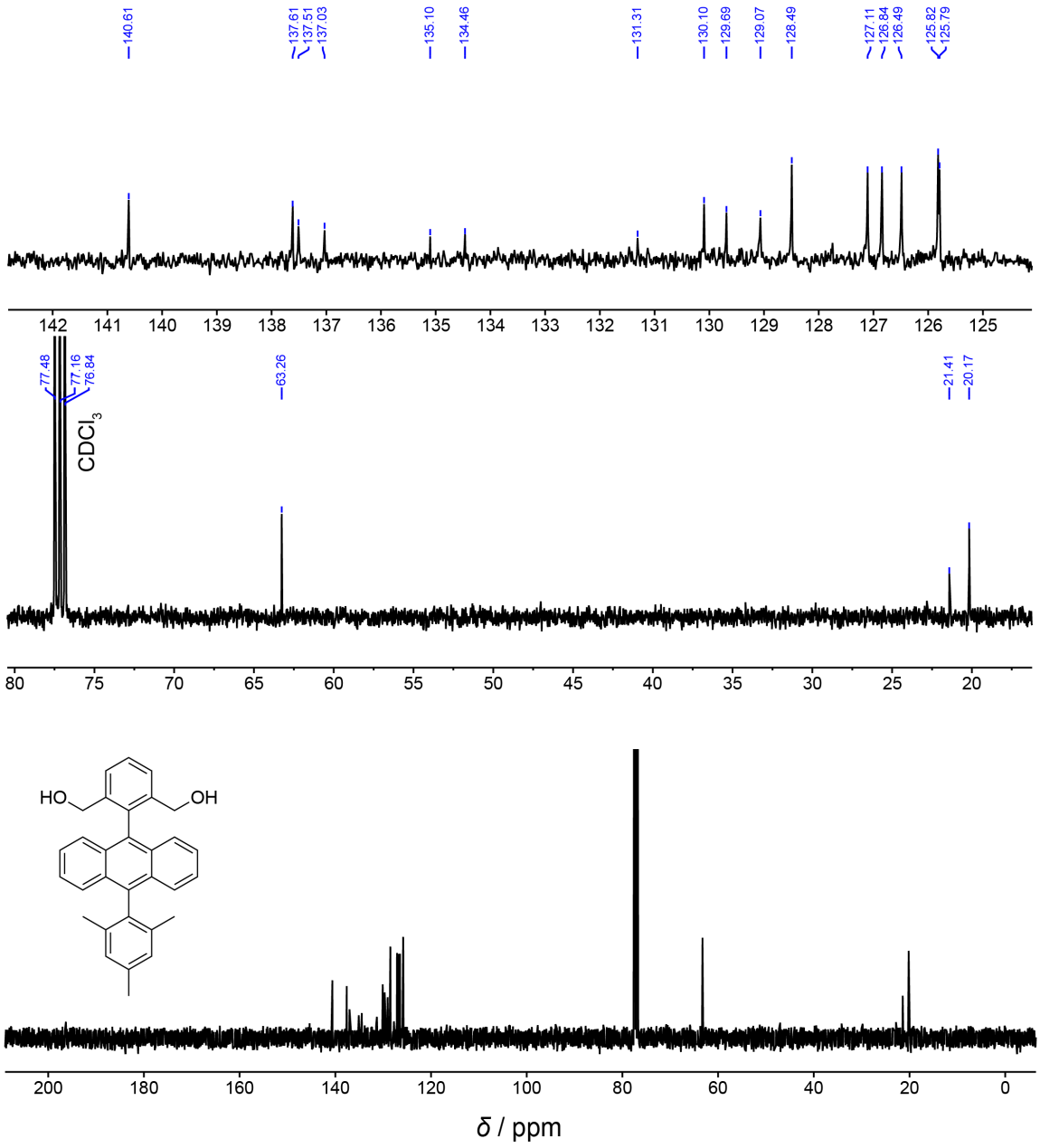

D:\Data\Service\Data\20_juQEx_1524 11/02/20 11:53:05 Sample: LV_420
Client: (+)-HR-ESI-MS Solvent: MeOH/CHCl3 3:2

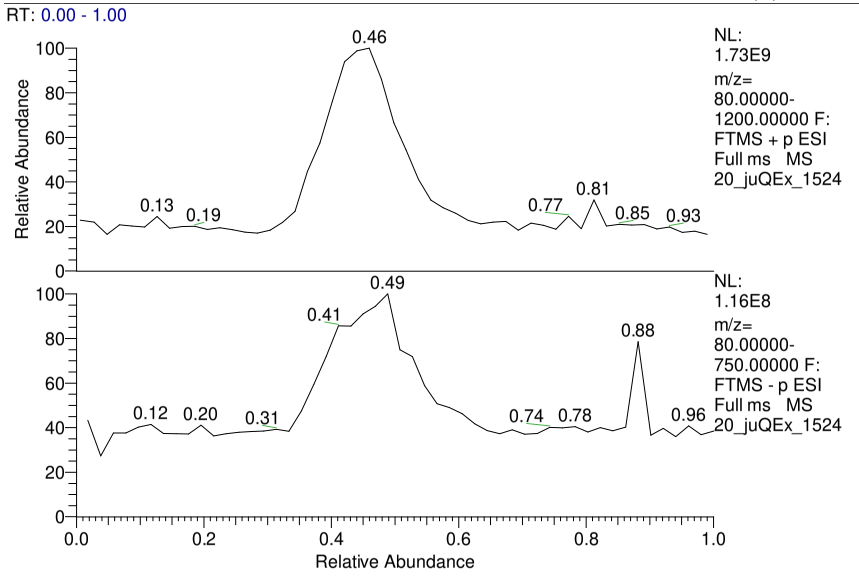

20_juQEx_1524#41-47 RT: 0.40-0.46 AV: 4
SB: 25 0.04-0.24 , 0.71-0.97
T: FTMS + p ESI Full lock ms [100.0000-1500.0000]
m/z= 454.86664-455.47783

m/z	Intensity	Relative	Theo. Mass	Delta (ppm)	RDB equiv.	Composition
455.19794	165025504.0	100.00	455.19787	0.16	21.5	$C_{29}H_{23}N_6$
			455.19815	-0.46	17.5	$C_{31}H_{28}O_2Na$
			455.19838	-0.97	3.5	$C_{16}H_{31}O_{11}N_4$
			455.19732	1.37	0.0	$C_{16}H_{34}O_{12}NNa$
			455.19866	-1.57	5.0	$C_{17}H_{30}O_8N_5Na$
			455.19681	2.49	18.0	$C_{29}H_{26}ON_3Na$
			455.19921	-2.79	21.0	$C_{31}H_{25}ON_3$
			455.19653	3.10	16.5	$C_{28}H_{27}O_4N_2$
			455.19973	-3.92	3.0	$C_{18}H_{33}O_{12}N$
			455.19598	4.32	0.5	$C_{14}H_{32}O_{11}N_4Na$
			455.20000	-4.52	4.5	$C_{19}H_{32}O_9N_2Na$

20_juQEx_1524 #40-47 RT: 0.40-0.46 AV: 4 SB: 25 0.03-0.24 , 0.70-0.95 NL: 2.45E8
T: FTMS + p ESI Full lock ms [100.0000-1500.0000]

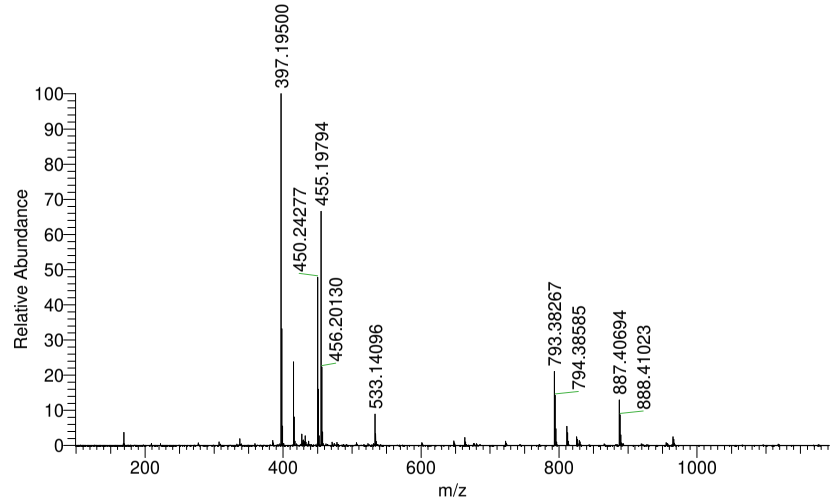

20_juQEx_1524 #40-46 RT: 0.40-0.44 AV: 3 SB: 25 0.03-0.24 , 0.70-0.95 NL: 1.54E8
T: FTMS + p ESI Full lock ms [100.0000-1500.0000]

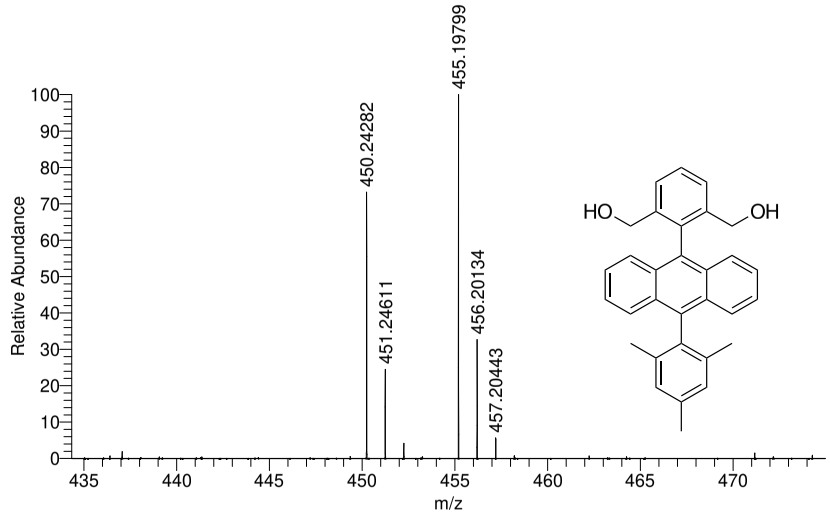

^{1}H NMR / 400 MHz / $CDCl_3$

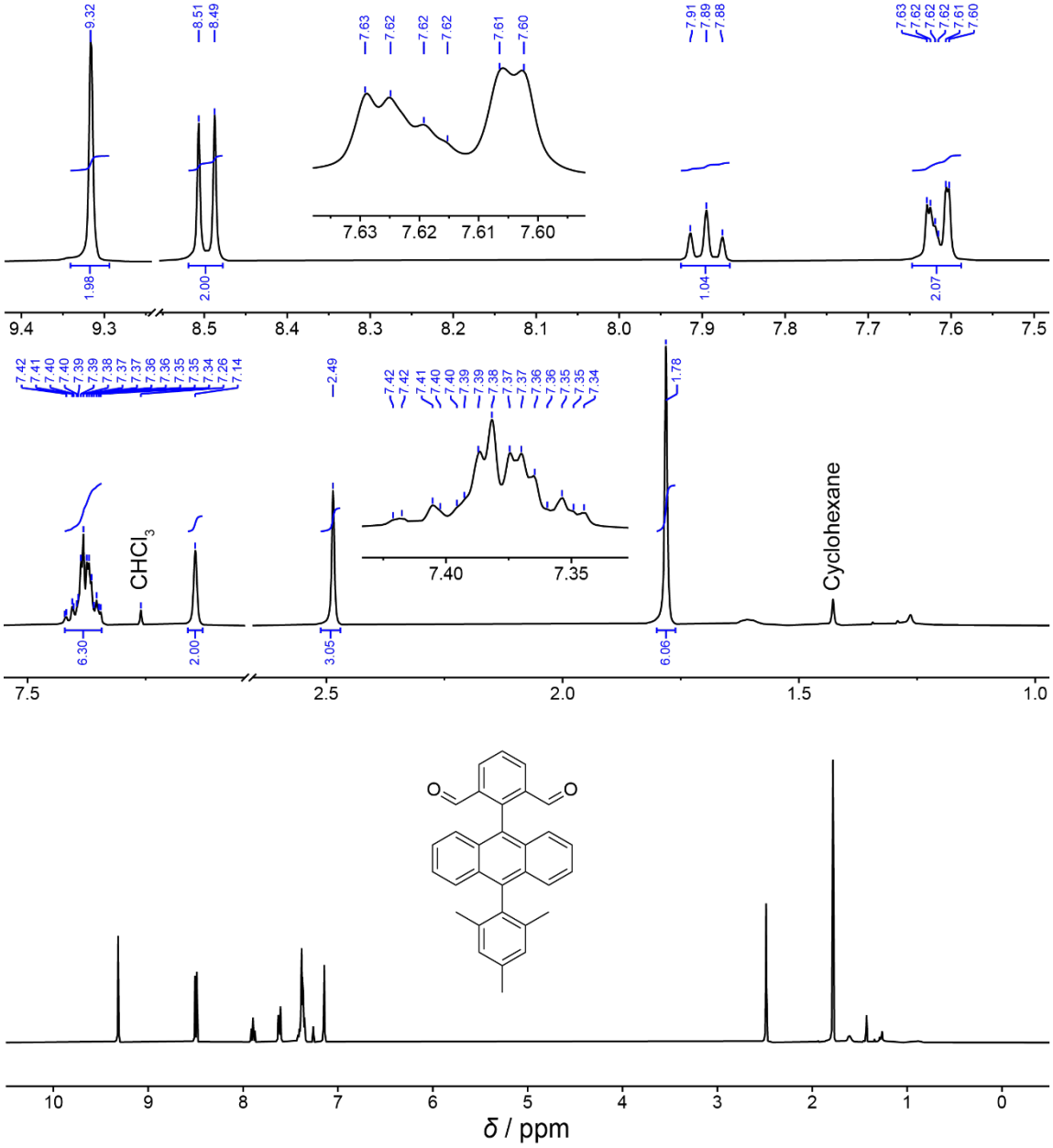

^{13}C NMR / 101 MHz / $CDCl_3$

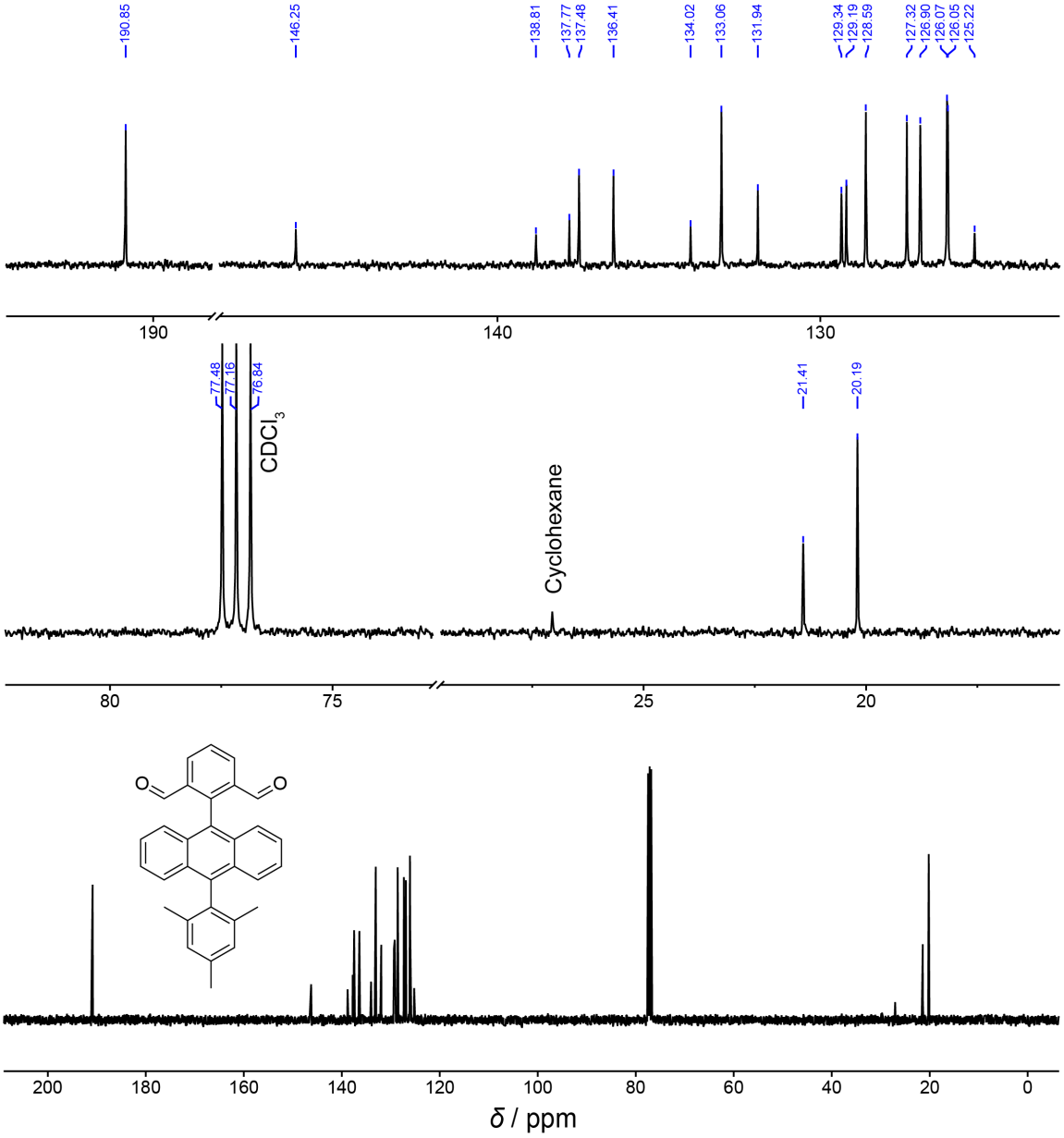

D:\Data\Service\Data\20_juQEx_1523 11/02/20 11:51:06 Sample: LV_421
Client: (+)-HR-ESI-MS Solvent: MeOH/CHCl3 3:2

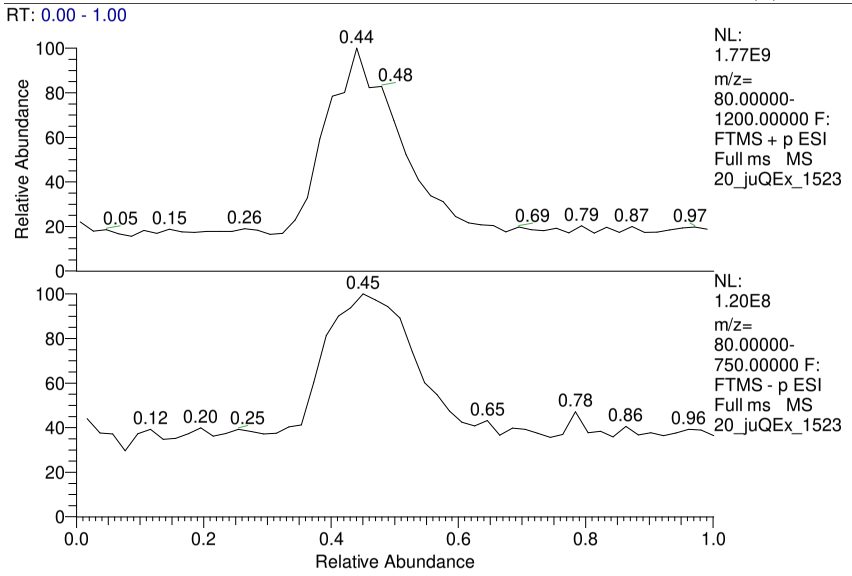

20_juQEx_1523#41-47 RT: 0.40-0.46 AV: 4
SB: 25 0.04-0.24 , 0.71-0.97
T: FTMS + p ESI Full lock ms [100.0000-1500.0000]
m/z= 428.56170-430.06154

m/z	Intensity	Relative	Theo. Mass	Delta (ppm)	RDB equiv.	Composition
429.18557	51130596.0	100.00	429.18541	0.36	7.0	$C_{17}H_{27}O_8N_5$
			429.18491	1.54	19.5	$C_{31}H_{25}O_2$
			429.18676	-2.77	6.5	$C_{19}H_{29}O_9N_2$
			429.18408	3.47	2.0	$C_{16}H_{31}O_{12}N$
			429.18356	4.67	20.0	$C_{29}H_{23}ON_3$

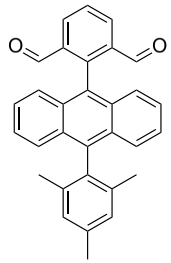

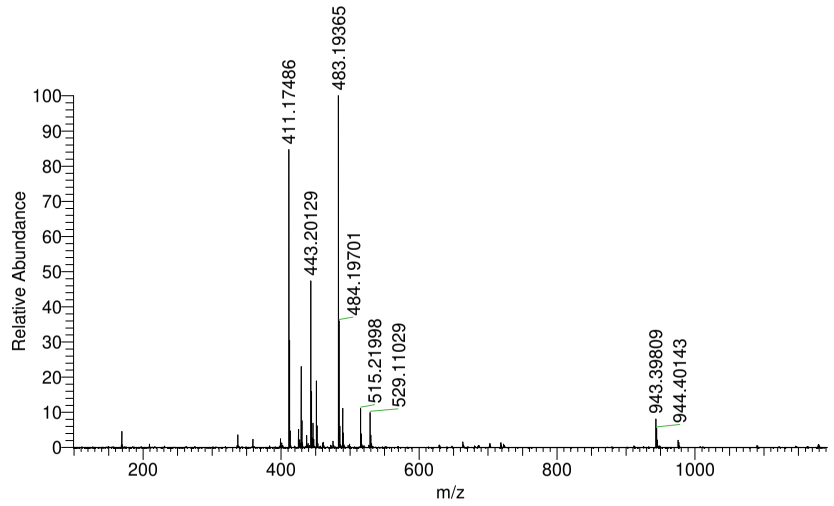

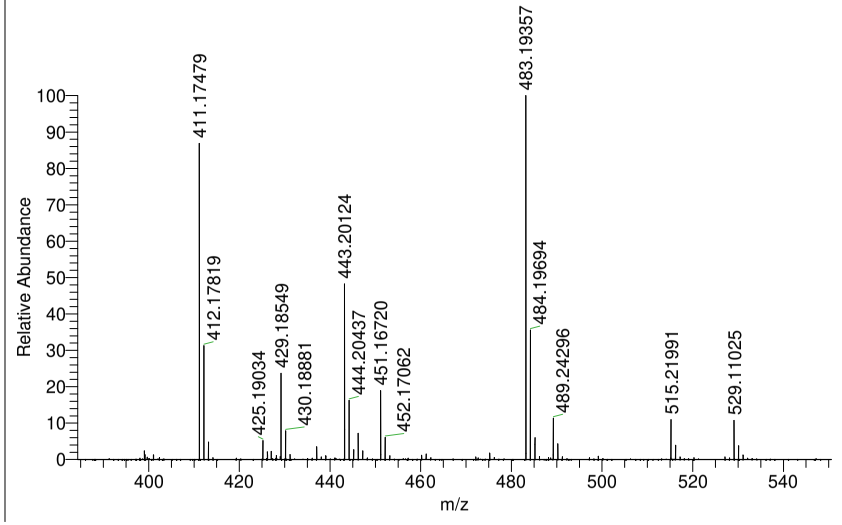

^{1}H NMR / 600 MHz / CD_2Cl_2

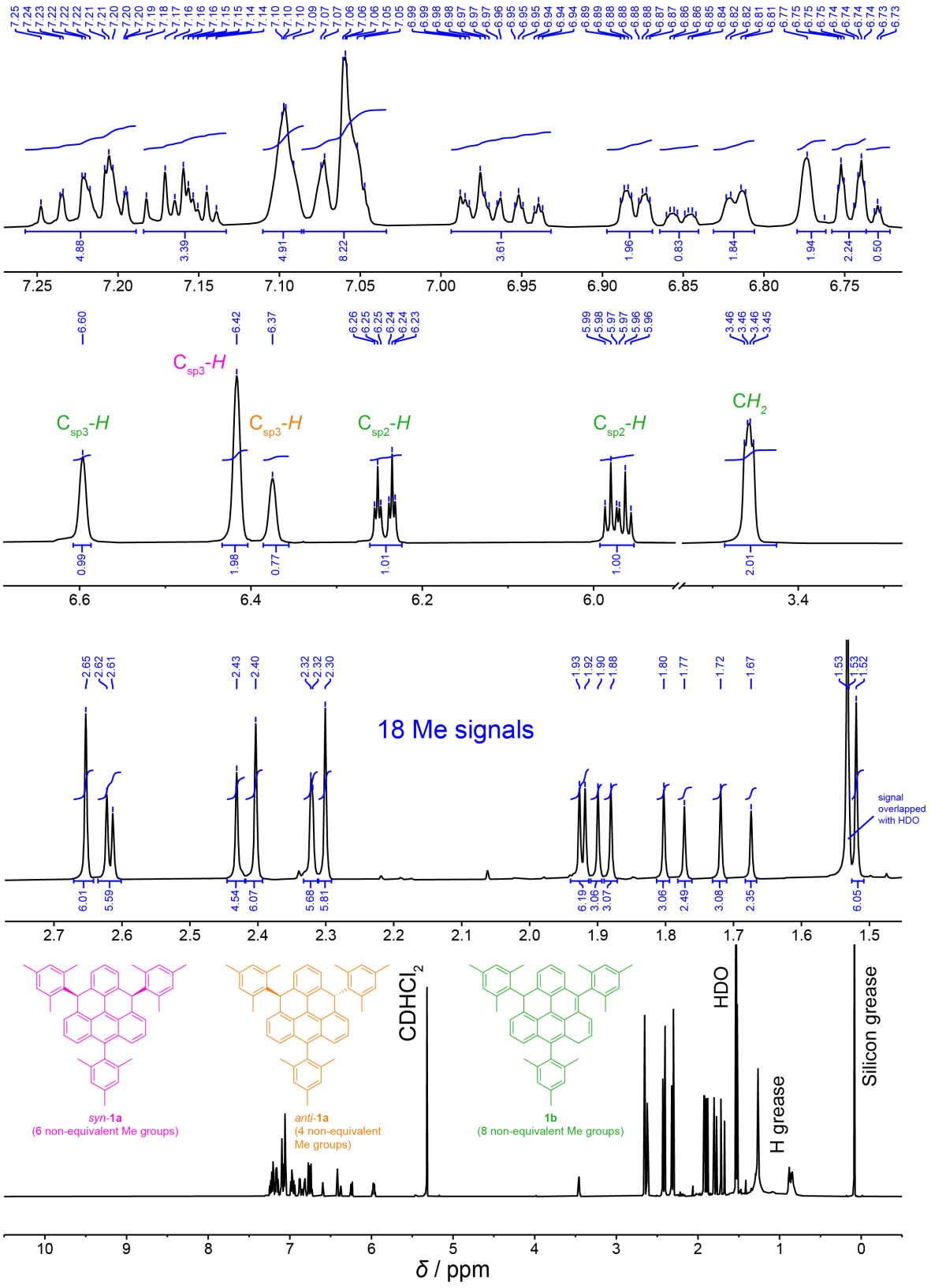

^{13}C NMR / 151 MHz / CD_2Cl_2

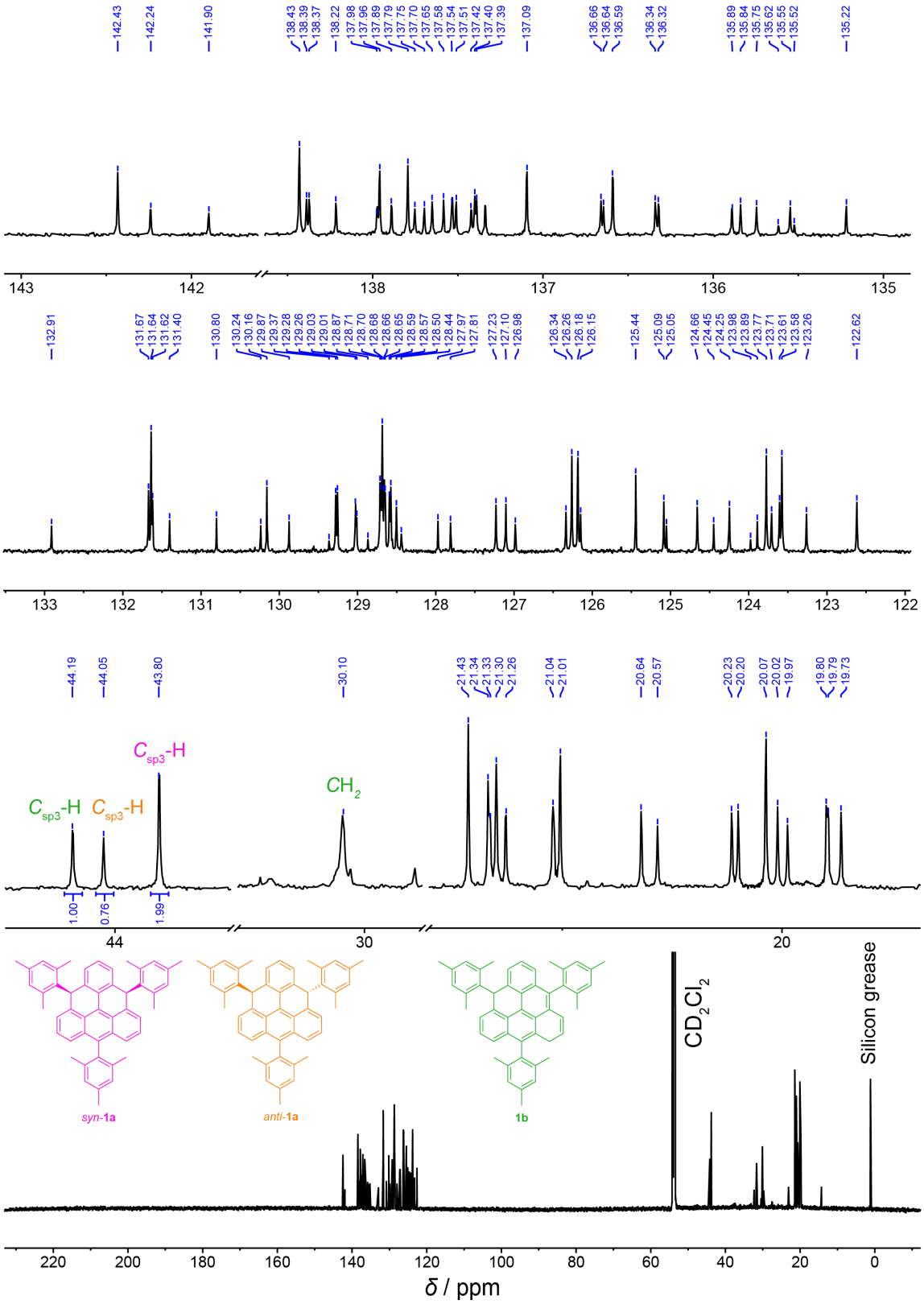

D:\Data\Service\Data\20_juQEx_1657 (+) HR-APCI-MS 11/18/20 12:59:05
Sample: LV_423 Comment: Client: Valenta Sheath liquid: MeOH + 0.1% HCOOH Solvent: DCM

20_juQEx_1657 #6-72 RT: 0.04-0.50 AV: 67 SB: 45 0.68-0.98 NL: 2.76E7
T: FTMS + p APCI corona Full lock ms [50.0000-750.0000]

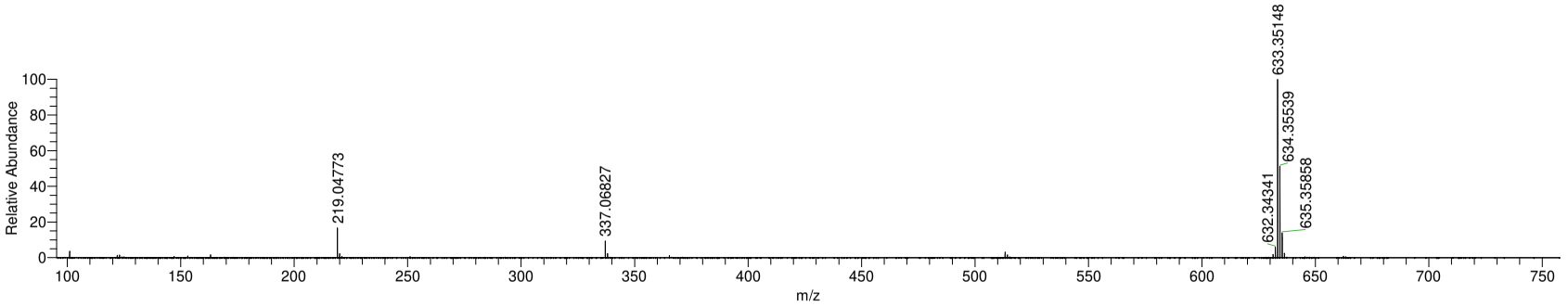

20_juQEx_1657 #6-72 RT: 0.04-0.50 AV: 67 SB: 45 0.68-0.98 NL: 2.76E7
T: FTMS + p APCI corona Full lock ms [50.0000-750.0000]

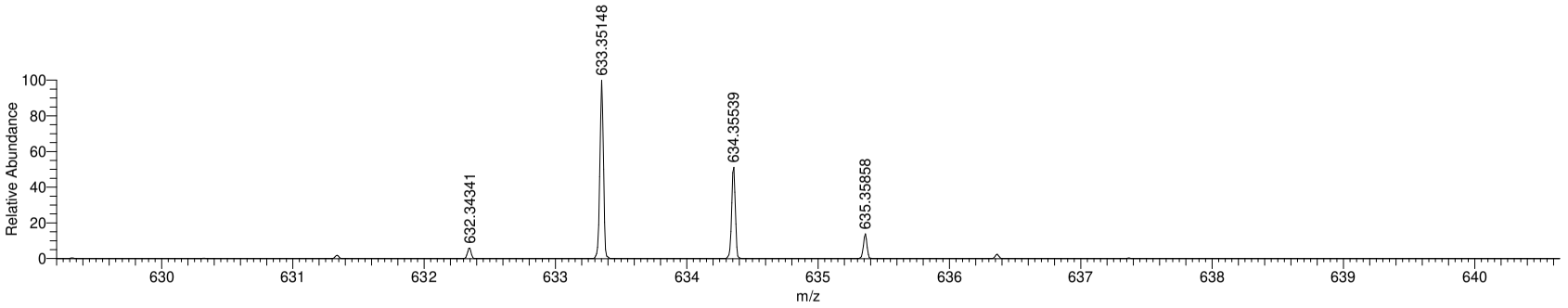

20_juQEx_1657#6-72 RT: 0.04-0.50 AV: 67
SB: 45 0.68-0.98
T: FTMS + p APCI corona Full lock ms [50.0000-750.0000]
m/z= 633.23691-633.44273

m/z	Intensity	Relative	Composition
633.35148	27597324.0	100.00	$C_{49}H_{45}$

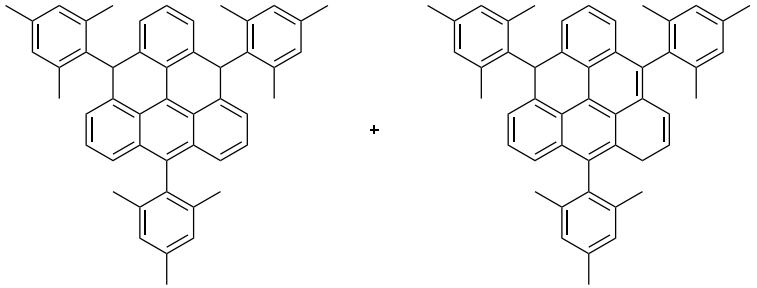

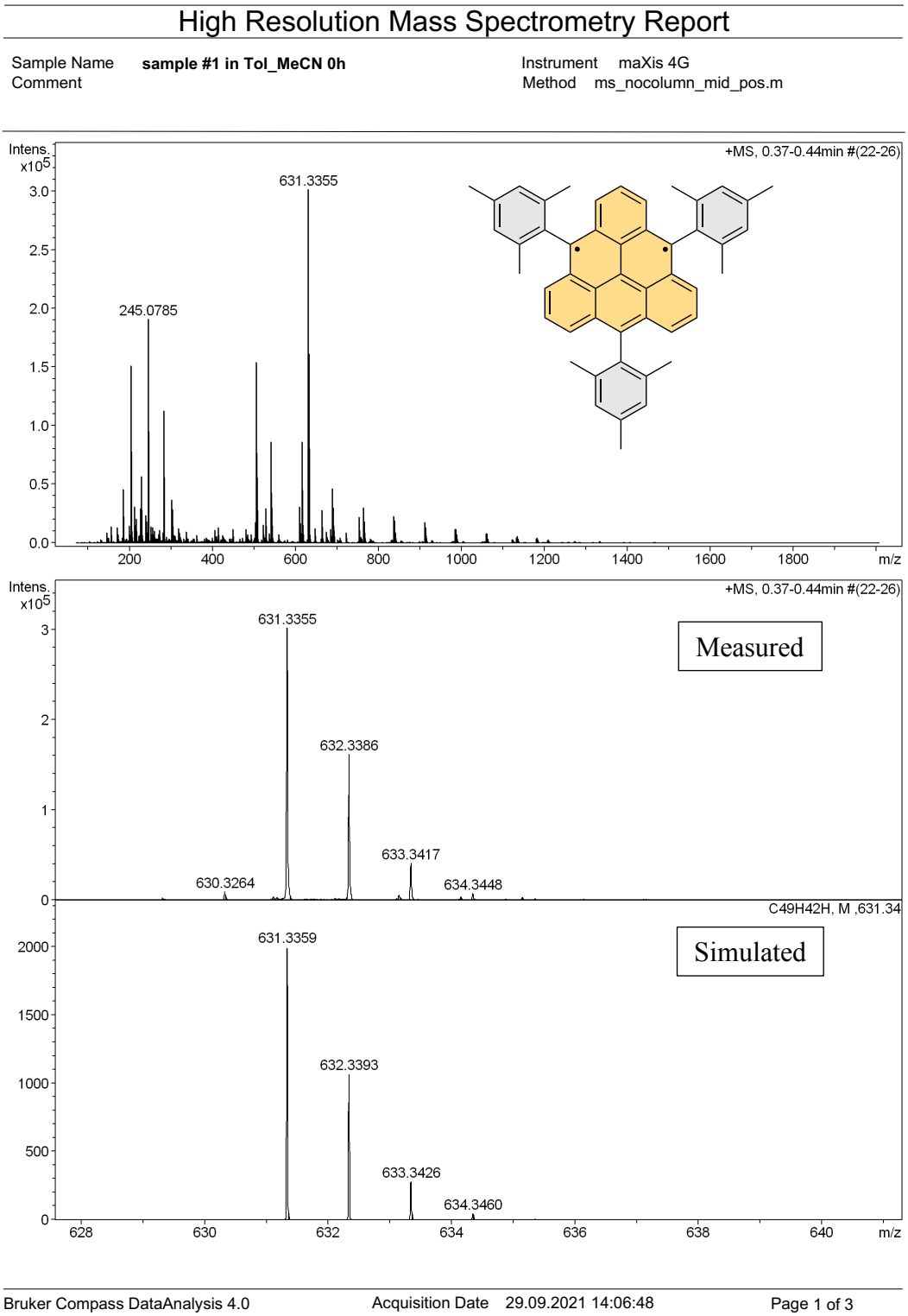

The sample of a 2.5 mM solution of **Mes_3-Tr** in toluene was evaporated to dryness using a Schlenk line, re-dissolved in acetonitrile, and measured. The desired $[M + H]^+ = 631.3555$ peak is observed and the isotopic distribution is in an agreement with the simulated pattern.

Measured m/z vs. theoretical m/z

Meas. m/z	#	Formula	Score	m/z	err [mDa]	err [ppm]	mSigma	rdb	e¯ Conf	z
631.3355	1	C 49 H 43	100.00	631.3359	0.4	0.7	2.0	28.5	even	1+

Mass list

#	m/z	I %	I
1	144.9820	2.9	8847
2	157.0834	4.6	13803
3	171.0991	4.6	13727
4	185.1146	15.2	45814
5	186.0084	2.8	8359
6	199.1302	5.0	15045
7	205.0599	50.2	151380
8	206.0634	3.5	10593
9	213.1459	10.3	31165
10	215.1251	4.9	14643
11	217.0468	4.6	13860
12	217.1046	6.8	20565
13	226.9514	2.9	8852
14	227.1251	9.7	29363
15	229.1409	18.9	56879
16	239.0887	7.9	23747
17	241.0679	6.2	18612
18	241.1771	2.4	7337
19	245.0785	63.3	190848
20	246.0816	8.6	26002
21	251.1250	4.8	14371
22	254.2474	2.4	7350
23	256.2631	4.4	13288
24	257.1357	2.4	7134
25	261.1305	3.5	10421
26	271.1875	2.4	7243
27	273.1669	3.6	10937
28	280.2631	3.0	9053
29	282.2789	37.5	112995
30	283.2820	7.2	21574
31	301.1406	12.2	36896
32	304.2606	9.6	28811
33	318.2398	4.3	12992
34	320.2552	3.1	9237
35	336.2503	3.3	9987
36	405.2603	3.6	10910
37	413.2654	4.4	13407
38	449.2863	4.1	12232
39	480.5128	3.9	11816
40	485.1120	2.4	7364
41	493.3122	2.6	7729
42	504.5125	5.9	17700
43	506.5288	51.1	153958
44	507.5319	18.7	56480
45	508.5386	4.9	14755
46	523.3234	5.2	15674
47	528.5102	9.9	29838
48	529.5138	3.7	11076
49	536.1643	2.7	8267
50	541.1202	28.6	86316
51	542.1206	13.6	40870
52	543.1181	10.0	30137
53	544.1180	3.4	10254
54	559.1301	2.5	7678
55	610.1829	10.2	30834
56	611.1837	5.7	17205
57	612.1819	4.4	13375
58	615.1388	28.5	86067
59	616.1395	16.4	49507
60	617.1368	11.5	34738
61	618.1366	5.1	15433
62	630.3264	3.2	9720

#	m/z	I %	I
63	526.4950	2.4	14383
64	528.5108	13.4	79209
65	529.5139	5.1	29923
66	530.5195	1.2	7346
67	535.5186	1.4	8103
68	537.5342	1.5	8984
69	557.5007	1.4	8491
70	559.5163	2.3	13599
71	561.5341	2.3	13650
72	563.5501	11.1	65806
73	564.5533	4.5	26747
74	565.5597	1.4	8264
75	585.5324	15.4	91097
76	586.5355	6.3	37117
77	587.5417	1.9	11446
78	613.4901	1.4	8165
79	615.5057	1.6	9396
80	617.5211	1.6	9269
81	631.3350	4.2	24929
82	631.5012	2.4	13952
83	632.3383	2.3	13617
84	633.5159	1.9	11019
85	645.4798	1.3	7822
86	647.4952	1.8	10466
87	649.5110	2.0	11642
88	663.4903	1.5	9160
89	679.4857	1.3	7717
90	783.7664	1.4	8226
91	787.8002	4.0	23418
92	788.8038	2.2	12837
93	807.7669	1.3	7823
94	809.7826	8.0	47251
95	810.7862	4.5	26551
96	811.7919	1.9	11187
97	823.7618	1.6	9232
98	825.7764	1.4	8550
99	841.7719	2.2	12900
100	842.7759	1.3	7677

Acquisition Parameter

General	Fore Vacuum	3.46e+000 mBar	High Vacuum	1.36e-007 mBar	Source Type	ESI
	Scan Begin	75 m/z	Scan End	1700 m/z	Ion Polarity	Positive
Source	Set Nebulizer	0.4 Bar	Set Capillary	3600 V	Set Dry Gas	4.0 l/min
	Set Dry Heater	180 °C	Set End Plate Offset	-500 V		
Quadrupole	Set Ion Energy (MS only)	4.0 eV				
Coll. Cell	Collision Energy	8.0 eV	Set Collision Cell RF	350.0 Vpp	100.0 Vpp	
Ion Cooler	Set Ion Cooler Transfer Time	75.0 µs	Set Ion Cooler Pre Pulse Storage Time	10.0 µs		

S8. Cartesian coordinates

1a′, E_{el} = –846.826514 Hartree

C	3.557730	1.202350	-0.074584
C	2.165225	1.215267	0.017674
C	1.450303	-0.000003	0.045274
C	2.165220	-1.215275	0.017674
C	3.557725	-1.202364	-0.074584
C	4.258826	-0.000008	-0.128761
C	-0.023222	0.000000	0.068403
C	-0.733462	-1.226213	0.047939
C	-0.733457	1.226216	0.047939
C	-0.053840	2.488060	0.047485
C	-0.779630	3.656498	-0.003988
C	-2.198162	3.649762	-0.039635
C	-2.879954	2.462456	-0.029992
C	-2.177087	1.220709	0.007136
C	-2.177092	-1.220700	0.007136
C	-2.879964	-2.462444	-0.029992
C	-2.198177	-3.649754	-0.039635
C	-0.779645	-3.656495	-0.003988
C	-0.053850	-2.488060	0.047485
C	-2.858070	0.000006	-0.007542
C	1.453581	2.543042	0.136023
C	1.453571	-2.543048	0.136023
H	4.096027	2.147570	-0.101464
H	4.096019	-2.147586	-0.101465
H	5.342681	-0.000010	-0.206406
H	-0.254136	4.609356	-0.011475
H	-2.736231	4.593281	-0.075309
H	-3.966636	2.442287	-0.056581
H	-3.966645	-2.442272	-0.056581
H	-2.736249	-4.593270	-0.075309
H	-0.254155	-4.609355	-0.011475

H	-3.945468	0.000008	-0.040896
H	1.841892	3.235311	-0.623604
H	1.732785	2.995540	1.100847
H	1.841880	-3.235319	-0.623604
H	1.732773	-2.995547	1.100847

1b′, E_{el} = –846.828300 Hartree

C	-0.550462	3.547950	0.091806
C	-0.595141	2.164069	0.039420
C	0.617550	1.426344	0.050974
C	1.861305	2.122762	0.116368
C	1.863476	3.536974	0.168545
C	0.675450	4.237598	0.156383
C	0.621015	-0.011405	-0.001920
C	1.843003	-0.712650	0.011241
C	-0.627281	-0.735462	-0.068489
C	-1.870799	-0.056958	-0.083163
C	-3.047750	-0.789817	-0.147787
C	-3.030148	-2.194634	-0.199057
C	-1.826640	-2.871711	-0.185599
C	-0.606320	-2.161276	-0.120412
C	1.840597	-2.157167	-0.042092
C	3.115750	-2.867335	-0.027559
C	4.294543	-2.233684	0.033420
C	4.412406	-0.738701	0.092308
C	3.087239	0.004463	0.077411
C	0.650160	-2.835950	-0.105149
C	-1.931019	1.454950	-0.029315
C	3.073085	1.373522	0.127444
H	-1.481052	4.111970	0.082843
H	2.815352	4.060177	0.218262
H	0.679618	5.323635	0.196511
H	-4.001317	-0.265710	-0.158908

H	-3.966650	-2.743688	-0.249221
H	-1.801441	-3.958042	-0.224882
H	3.077850	-3.953988	-0.068822
H	5.221926	-2.802269	0.042071
H	5.036836	-0.392335	-0.746796
H	4.981300	-0.456482	0.992692
H	0.653905	-3.923432	-0.145110
H	-2.540334	1.756461	0.835347
H	-2.484851	1.820718	-0.906409
H	4.013040	1.921104	0.177644

syn-**1a**, E_{el} = –1893.817329 Hartree

C	2.333637	3.680572	1.208025
C	2.174755	3.692545	-0.198553
C	2.703929	4.769248	-0.941216
C	3.375150	5.804184	-0.275059
C	3.539429	5.809398	1.108926
C	3.010545	4.733659	1.828388
C	1.439250	2.553898	-0.917839
C	2.162043	1.214272	-0.835111
C	1.444846	-0.001507	-0.770423
C	-0.019818	-0.000148	-0.605926
C	-0.723993	1.225569	-0.495088
C	-0.046201	2.488825	-0.581125
C	-0.726209	-1.224536	-0.494588
C	-0.050706	-2.489061	-0.580073
C	1.434584	-2.556934	-0.916992
C	2.159823	-1.218612	-0.834706
C	3.554848	1.198471	-0.939358
C	4.253445	-0.004105	-0.984154
C	3.552642	-1.205383	-0.939133
C	-2.153054	1.222455	-0.269339
C	-2.854050	0.002515	-0.162685

C	-2.155253	-1.218733	-0.268726
C	-2.841126	-2.467699	-0.147817
C	-2.162266	-3.652860	-0.229681
C	-0.762523	-3.659981	-0.443122
C	-2.836716	2.472714	-0.149204
C	-2.155728	3.656615	-0.231786
C	-0.755959	3.661099	-0.445081
C	-4.337908	0.003671	0.067189
C	-5.224682	0.006589	-1.030658
C	-6.603552	0.011312	-0.794462
C	-7.132375	0.010362	0.499043
C	-6.237709	0.011525	1.572631
C	-4.851931	0.006799	1.381604
C	-4.704970	0.009039	-2.451079
C	-8.625640	-0.017058	0.729974
C	-3.927623	0.009449	2.578770
C	2.577722	4.856118	-2.450667
C	4.248358	6.942209	1.813985
C	1.795060	2.560817	2.070555
H	4.093171	2.140585	-0.979367
H	4.089172	-2.148519	-0.979147
H	5.337410	-0.005094	-1.061717
H	-0.230523	4.609984	-0.497905
H	-2.684414	4.601040	-0.132584
H	-3.908641	2.463996	0.014047
H	-3.913010	-2.456876	0.015518
H	-2.692587	-4.596295	-0.129771
H	-0.238811	-4.609856	-0.495201
H	1.465256	2.799117	-1.987775
H	1.460087	-2.802392	-1.986891
C	2.168453	-3.696560	-0.197601
H	-7.281509	0.017177	-1.646138
H	-6.626926	0.017573	2.589240

H	3.779623	6.627589	-0.860529
H	3.128040	4.710557	2.910452
H	-3.273820	-0.870595	2.583609
H	-3.273796	0.889497	2.580324
H	-4.498478	0.011145	3.512575
H	-5.531160	0.010530	-3.168919
H	-4.082105	0.889015	-2.650197
H	-4.082947	-0.870881	-2.653014
H	-8.896244	0.484173	1.665623
H	-9.166933	0.473692	-0.086111
H	-9.000652	-1.047548	0.794207
H	4.976524	6.567983	2.543258
H	4.781440	7.583710	1.104819
H	3.540460	7.576046	2.364265
H	2.230552	1.593174	1.798155
H	2.022130	2.745870	3.125053
H	0.708671	2.460960	1.973142
H	3.048455	5.772326	-2.819929
H	3.063532	4.013548	-2.958713
H	1.531258	4.872737	-2.780269
C	2.327901	-3.684387	1.208916
C	3.000401	-4.740039	1.829707
C	3.527364	-5.816812	1.110374
C	3.357858	-5.814447	-0.272987
C	2.690912	-4.777014	-0.939559
C	1.790150	-2.564232	2.071443
H	3.114274	-4.719097	2.912202
C	4.266160	-6.932673	1.811789
H	3.753666	-6.642727	-0.857498
C	2.557526	-4.867823	-2.448161
H	2.017366	-2.749289	3.125909
H	2.226468	-1.597029	1.798806
H	0.703833	-2.463393	1.974247

H	3.046414	-4.029734	-2.960666
H	3.021287	-5.787898	-2.816630
H	1.509655	-4.879000	-2.773465
H	4.425135	-7.787457	1.146445
H	5.251966	-6.600507	2.163245
H	3.715896	-7.287771	2.691130

anti-**1a**, E_{el} = –1893.817395 Hartree

C	2.351157	3.982119	1.105279
C	2.287690	3.669874	-0.274020
C	2.889365	4.542741	-1.205105
C	3.538203	5.698761	-0.749043
C	3.609504	6.022187	0.604745
C	3.008521	5.145600	1.513031
C	1.575331	2.401679	-0.762454
C	2.255452	1.113275	-0.313660
C	1.504602	-0.041560	0.000948
C	0.031712	-0.000928	0.000427
C	-0.648593	1.216533	-0.253208
C	0.067833	2.428866	-0.535727
C	-0.714859	-1.179003	0.253684
C	-0.066562	-2.429069	0.536318
C	1.440054	-2.485219	0.763673
C	2.190413	-1.235980	0.316155
C	3.651222	1.060542	-0.309965
C	4.319956	-0.119090	0.002460
C	3.586980	-1.260137	0.314018
C	-2.093951	1.259546	-0.216290
C	-2.835062	0.078246	-0.000175
C	-2.160380	-1.142166	0.216173
C	-2.887201	-2.357761	0.414082
C	-2.233263	-3.537537	0.643982
C	-0.818962	-3.568935	0.712089

C	-2.752505	2.513384	-0.414617
C	-2.034340	3.655208	-0.644508
C	-0.620441	3.608469	-0.712093
C	-4.335998	0.119484	-0.000397
C	-5.049642	-0.054930	-1.205410
C	-6.447680	-0.009763	-1.183527
C	-7.162462	0.201790	-0.001498
C	-6.437337	0.376826	1.180239
C	-5.039167	0.337779	1.203661
C	-4.325038	-0.285316	-2.512895
C	-8.673660	0.215323	0.002971
C	-4.303121	0.534033	2.510323
C	2.864673	4.280619	-2.699255
C	4.295707	7.282091	1.078807
C	1.731833	3.094695	2.162165
H	4.215323	1.957655	-0.546652
H	4.100585	-2.186964	0.551204
H	5.406269	-0.148991	0.003086
H	-0.068161	4.522324	-0.909517
H	-2.544870	4.604160	-0.786499
H	-3.835880	2.541764	-0.378253
H	-3.970468	-2.326196	0.377294
H	-2.795439	-4.456900	0.785578
H	-0.318032	-4.511934	0.909446
H	1.682170	2.390515	-1.855282
C	2.081491	-3.790395	0.274331
H	1.546938	-2.480934	1.856540
H	-6.991346	-0.142272	-2.117272
H	-6.972828	0.549976	2.112060
H	3.999329	6.362212	-1.478122
H	3.051806	5.372690	2.576879
H	-3.626494	1.395511	2.465801
H	-5.005810	0.698484	3.333162

H	-3.688220	-0.338615	2.760002
H	-5.035452	-0.408880	-3.336257
H	-3.663885	0.553720	-2.759604
H	-3.695921	-1.182209	-2.471335
H	-9.066789	0.861271	0.795491
H	-9.074579	0.569540	-0.952876
H	-9.081250	-0.790527	0.172681
H	4.969589	7.080006	1.919768
H	4.884590	7.742241	0.278760
H	3.567820	8.028347	1.423648
H	2.183878	2.096840	2.169362
H	1.866985	3.531433	3.156564
H	0.657632	2.957687	1.998285
H	3.377589	5.084879	-3.235412
H	3.365229	3.341320	-2.966172
H	1.842621	4.226350	-3.094750
C	2.632564	-4.696595	1.204904
C	3.216520	-5.886379	0.748000
C	3.271176	-6.211595	-0.606140
C	2.720998	-5.301745	-1.513899
C	2.129062	-4.103935	-1.105305
C	2.620807	-4.435394	2.699375
H	3.639158	-6.575402	1.476687
C	3.886444	-7.507290	-1.081101
H	2.752743	-5.529563	-2.577999
C	1.561784	-3.181826	-2.161712
H	3.118204	-8.212134	-1.425560
H	4.569789	-7.342433	-1.922536
H	4.449627	-7.999522	-0.281643
H	3.087315	-5.267758	3.235025
H	3.172800	-3.525900	2.968091
H	1.602930	-4.324539	3.093822
H	2.071737	-2.212270	-2.169481

H	1.670094	-3.625832	-3.156179
H	0.497674	-2.981868	-1.996845

1b, E_{el} = –1893.826979 Hartree

C	-2.649728	-0.987746	-0.085497
C	-2.443577	0.425815	-0.255801
C	-1.115801	0.935352	-0.389592
C	-0.000039	0.028823	-0.314835
C	-0.226732	-1.349252	-0.131724
C	-1.573986	-1.851309	-0.032201
C	-3.536159	1.327917	-0.299741
C	-3.324204	2.679749	-0.466084
C	-2.017624	3.178955	-0.604807
C	-0.920827	2.331947	-0.574521
C	1.351525	0.532038	-0.390815
C	1.609863	1.915811	-0.576622
C	0.470842	2.895008	-0.848967
C	2.448397	-0.373939	-0.258143
C	2.197913	-1.782565	-0.085528
C	0.899455	-2.256270	-0.030714
C	-1.832397	-3.338910	0.139914
C	-0.603751	-4.186629	0.216461
C	0.634579	-3.683952	0.140184
C	3.769616	0.134523	-0.304699
C	3.999305	1.484438	-0.473834
C	2.920416	2.371721	-0.611376
H	-1.862440	4.246091	-0.733358
H	-4.543762	0.939173	-0.199152
H	-4.167539	3.364830	-0.493611
H	3.110987	3.432814	-0.742039
H	5.017039	1.864665	-0.503905
H	4.601770	-0.553531	-0.204279
H	1.493243	-4.344052	0.204554

H	-0.750353	-5.257481	0.341606
H	-2.446278	-3.507181	1.038316
H	-2.472264	-3.700234	-0.680689
C	3.366475	-2.719778	0.032180
H	0.493068	3.032739	-1.937879
C	0.699102	4.282120	-0.234903
C	-4.050270	-1.517362	0.031738
C	-4.762513	-1.899692	-1.124680
C	-6.061966	-2.400717	-0.992052
C	-6.679468	-2.534031	0.254481
C	-5.962722	-2.136411	1.386407
C	-4.661369	-1.630592	1.298567
C	-4.148939	-1.757450	-2.500287
H	-6.606790	-2.690337	-1.888879
C	-8.071631	-3.109169	0.376576
H	-6.429213	-2.217387	2.366632
C	-3.937208	-1.197248	2.554277
C	3.915203	-3.012399	1.298898
C	5.012594	-3.875772	1.384776
C	5.583249	-4.461435	0.251513
C	5.028261	-4.155384	-0.993997
C	3.931494	-3.296914	-1.124992
C	3.333300	-2.408320	2.557519
H	5.432771	-4.094150	2.364974
C	6.748833	-5.415897	0.371362
H	5.460707	-4.594599	-1.891278
C	3.367321	-3.001596	-2.496909
H	-8.600599	-2.699101	1.243690
H	-8.671566	-2.900829	-0.515879
H	-8.043121	-4.200251	0.500585
H	-2.997071	-1.744111	2.693868
H	-3.677396	-0.132580	2.519062
H	-4.557880	-1.364081	3.440106

H	-4.836495	-2.114676	-3.273223
H	-3.903888	-0.712089	-2.722674
H	-3.214715	-2.324089	-2.592435
H	7.385143	-5.386094	-0.519759
H	7.372235	-5.180753	1.240808
H	6.405263	-6.452542	0.489737
H	3.910178	-2.709231	3.437624
H	3.328025	-1.313024	2.513743
H	2.294307	-2.723477	2.711249
H	3.370288	-1.926498	-2.710872
H	3.950905	-3.503301	-3.275138
H	2.327478	-3.338354	-2.584996
C	0.730757	4.458758	1.169167
C	0.939022	5.737479	1.692584
C	1.120723	6.858462	0.877386
C	1.083263	6.666771	-0.502713
C	0.877390	5.403065	-1.073324
C	0.543329	3.306544	2.131110
H	0.958568	5.859745	2.774179
C	1.366283	8.223706	1.476361
H	1.217030	7.522865	-1.161206
C	0.852769	5.298712	-2.586701
H	0.601365	3.657955	3.165985
H	-0.428123	2.818904	1.995830
H	1.309410	2.535626	1.994681
H	-0.104473	4.915764	-2.962262
H	1.008053	6.283045	-3.038770
H	1.639086	4.636869	-2.971035
H	1.240637	9.016144	0.731396
H	0.678786	8.427876	2.305507
H	2.385404	8.307086	1.876783

8a′, E_{el} = –846.215774 Hartree

C	2.234066	3.016926	-0.067709
C	1.837711	1.656347	-0.057702
C	0.434248	1.349774	-0.037035
C	-0.526441	2.400471	-0.026864
C	-0.076146	3.743570	-0.037430
C	1.285540	4.036601	-0.057563
C	-0.002314	-0.005607	-0.026644
C	-1.393731	-0.306631	-0.006198
C	0.960048	-1.061034	-0.036672
C	2.361666	-0.754387	-0.057314
C	3.290465	-1.825108	-0.066966
C	2.855075	-3.146224	-0.056530
C	1.493585	-3.447806	-0.036400
C	0.526244	-2.417397	-0.026185
C	-1.814850	-1.682195	0.004200
C	-3.245473	-1.975599	0.025182
C	-4.175843	-1.011311	0.035047
C	-3.836268	0.451972	0.025481
C	-2.347912	0.755450	0.003794
C	-0.874131	-2.687905	-0.005699
C	2.768752	0.597446	-0.067383
C	-1.908840	2.061371	-0.006438
H	3.294560	3.255014	-0.083515
H	-0.809478	4.545927	-0.029589
H	1.611964	5.073249	-0.065463
H	4.353436	-1.598227	-0.082728
H	3.583759	-3.952556	-0.064150
H	1.162053	-4.483039	-0.028330
H	-3.539102	-3.023210	0.032730
H	-5.232135	-1.270816	0.050670
H	-4.298142	0.935661	0.901114
H	-4.322275	0.929812	-0.840245

H	-1.201082	-3.725784	0.002280
H	3.831577	0.828168	-0.082741
H	-2.636165	2.871721	0.001242

8b′, E_{el} = –846.219465 Hartree

C	2.198123	3.034445	-0.004917
C	1.824428	1.698795	-0.004591
C	0.449167	1.357474	-0.025644
C	-0.534902	2.400788	-0.047039
C	-0.106545	3.754896	-0.046576
C	1.235498	4.063706	-0.025868
C	0.021318	-0.018490	-0.026027
C	-1.352389	-0.325363	-0.047201
C	0.993647	-1.081687	-0.004837
C	2.383431	-0.805300	0.016721
C	3.289611	-1.855049	0.036634
C	2.856189	-3.196211	0.035969
C	1.510322	-3.487846	0.015294
C	0.546879	-2.444631	-0.005594
C	-1.793709	-1.699568	-0.047866
C	-3.190003	-1.975601	-0.069618
C	-4.124819	-0.944780	-0.090317
C	-3.717350	0.386016	-0.089836
C	-2.336316	0.730387	-0.068531
C	-0.838114	-2.719908	-0.027063
C	2.889060	0.622144	0.018253
C	-1.905337	2.060512	-0.068009
H	3.255188	3.291765	0.011316
H	-0.857232	4.541130	-0.062867
H	1.558751	5.101248	-0.025587
H	4.355703	-1.638138	0.053114
H	3.589991	-3.997616	0.051849
H	1.165267	-4.518834	0.014586

H	-3.516278	-3.012325	-0.069463
H	-5.185370	-1.181813	-0.106603
H	-4.453567	1.185401	-0.105652
H	-1.167817	-3.756534	-0.027425
H	3.557753	0.764107	-0.843341
H	3.528764	0.772465	0.900202
H	-2.644664	2.858263	-0.084219

8a, E_{el} = –1893.223777 Hartree

C	2.201126	1.790569	-0.000049
C	0.862575	2.313992	-0.000062
C	-0.242577	1.412577	-0.000047
C	-0.008080	0.007646	-0.000029
C	1.323558	-0.493678	-0.000033
C	2.424288	0.421260	-0.000042
C	0.610009	3.708751	-0.000084
C	-0.692842	4.195672	-0.000096
C	-1.778735	3.327089	-0.000077
C	-1.588505	1.921702	-0.000046
C	-1.114005	-0.895488	-0.000002
C	-2.458702	-0.387096	0.000015
C	-2.689205	1.019251	-0.000009
C	-0.881623	-2.303230	0.000015
C	0.470436	-2.801526	0.000000
C	1.541810	-1.919177	-0.000022
C	3.852260	-0.097704	-0.000039
C	3.976924	-1.588665	-0.000038
C	2.919709	-2.410408	-0.000031
C	-1.992887	-3.179226	0.000051
C	-3.293363	-2.682445	0.000075
C	-3.532264	-1.314097	0.000059
H	-2.789606	3.719924	-0.000083
H	1.448392	4.396746	-0.000094

H	-0.864699	5.268983	-0.000118
H	-4.549746	-0.938775	0.000083
H	-4.131830	-3.374147	0.000107
H	-1.820574	-4.249781	0.000064
H	3.066251	-3.485512	-0.000030
H	4.984888	-1.998348	-0.000043
H	4.396510	0.312563	-0.865124
H	4.396507	0.312565	0.865048
C	0.697273	-4.286453	0.000011
C	-4.091863	1.548161	0.000017
C	3.362690	2.741933	-0.000027
C	0.800617	-4.987473	-1.220385
C	1.005303	-6.371170	-1.197606
C	1.107104	-7.084096	0.000032
C	1.005350	-6.371145	1.197660
C	0.800665	-4.987447	1.220418
C	0.703303	-4.263281	-2.544705
H	1.088051	-6.904779	-2.142812
C	1.295049	-8.583629	0.000045
H	1.088136	-6.904734	2.142874
C	0.703402	-4.263228	2.544726
C	-4.754033	1.800430	-1.220690
C	-6.061394	2.297423	-1.197712
C	-6.735625	2.550126	0.000057
C	-6.061281	2.297653	1.197778
C	-4.753896	1.800648	1.220721
C	-4.068274	1.544945	-2.544352
H	-6.564708	2.493034	-2.142915
C	-8.159502	3.056523	0.000017
H	-6.564498	2.493438	2.142992
C	-4.068031	1.545397	2.544373
C	3.909813	3.192211	1.220233
C	4.999329	4.069447	1.197637

C	5.564509	4.515932	0.000030
C	4.999370	4.069476	-1.197601
C	3.909850	3.192239	-1.220254
C	3.324108	2.755215	2.545008
H	5.413981	4.415590	2.142747
C	6.762627	5.436955	0.000075
H	5.414057	4.415637	-2.142689
C	3.324183	2.755284	-2.545059
H	-0.241141	-3.714300	2.634965
H	0.766637	-4.967452	3.380161
H	1.508484	-3.527929	2.661606
H	1.844405	-8.919156	0.886315
H	0.329177	-9.106835	0.000069
H	1.844370	-8.919175	-0.886241
H	0.766505	-4.967524	-3.380127
H	-0.241244	-3.714355	-2.634919
H	1.508380	-3.527986	-2.661633
H	-3.153963	2.142308	2.645532
H	-4.728350	1.794596	3.380860
H	-3.772874	0.494595	2.647943
H	-4.728643	1.794044	-3.380830
H	-3.154188	2.141801	-2.645666
H	-3.773169	0.494115	-2.647781
H	-8.369740	3.662867	0.887684
H	-8.368066	3.667482	-0.884896
H	-8.878294	2.225877	-0.002875
H	6.774300	6.080232	-0.886410
H	6.773747	6.080865	0.886110
H	7.702638	4.868622	0.000580
H	3.882904	3.187952	3.380601
H	2.277051	3.066106	2.641568
H	3.338209	1.664732	2.659164
H	3.338172	1.664799	-2.659199

H	2.277165	3.066287	-2.641689
H	3.883075	3.187952	-3.380624

8b, E_{el} = –1893.219439 Hartree

C	2.484574	-1.391885	-0.083771
C	2.486692	0.023062	-0.257010
C	1.246986	0.735959	-0.389685
C	0.000109	0.017935	-0.311508
C	0.008277	-1.377285	-0.123698
C	1.260960	-2.093448	-0.022682
C	3.706305	0.754150	-0.307570
C	3.701922	2.119731	-0.478170
C	2.485203	2.813038	-0.615325
C	1.270962	2.143452	-0.578862
C	-1.255099	0.721258	-0.390006
C	-1.295563	2.128350	-0.579315
C	-0.016854	2.916714	-0.851496
C	-2.486385	-0.006152	-0.257679
C	-2.467691	-1.420965	-0.084344
C	-1.235936	-2.108105	-0.022942
C	1.229542	-3.507380	0.147463
C	0.024781	-4.195280	0.225652
C	-1.187956	-3.521567	0.147231
C	-3.714495	0.710533	-0.308763
C	-3.726121	2.076034	-0.479691
C	-2.517592	2.783575	-0.616519
H	2.494583	3.890839	-0.747202
H	4.642674	0.216316	-0.207755
H	4.639549	2.668424	-0.510451
H	-2.539548	3.861140	-0.748844
H	-4.670139	2.613628	-0.512521
H	-4.644507	0.161738	-0.209192
H	-2.120524	-4.070058	0.217672

H	0.031103	-5.274584	0.354669
H	2.168468	-4.044889	0.218087
C	-3.758939	-2.175692	0.032650
C	-0.025412	4.321725	-0.235709
H	-0.017560	3.057321	-1.940184
C	3.784568	-2.131402	0.033505
C	-4.394061	-2.676551	-1.123975
C	-5.596405	-3.379289	-0.992093
C	-6.192221	-3.598616	0.252853
C	-5.545816	-3.097748	1.386134
C	-4.342265	-2.390030	1.299875
C	-3.790317	-2.468299	-2.495026
H	-6.078681	-3.766102	-1.888067
C	-7.508354	-4.332409	0.367738
H	-5.988247	-3.262225	2.367042
C	-3.682375	-1.870930	2.557927
C	4.370072	-2.338938	1.300869
C	5.581824	-3.032466	1.387384
C	6.234342	-3.525658	0.254227
C	5.636295	-3.313284	-0.990843
C	4.425802	-2.624706	-1.122984
C	3.703844	-1.827647	2.558779
H	6.025920	-3.191785	2.368394
C	7.558954	-4.243975	0.369448
H	6.123298	-3.694361	-1.886716
C	3.819997	-2.423479	-2.494174
H	-3.557487	-0.782167	2.526665
H	-4.279007	-2.117095	3.441809
H	-2.682843	-2.300320	2.694381
H	-4.419134	-2.916406	-3.270664
H	-3.675803	-1.402743	-2.726228
H	-2.792510	-2.916806	-2.567673
H	-7.591494	-4.859928	1.324105

H	-8.358278	-3.639362	0.304868
H	-7.629844	-5.066673	-0.435950
H	4.302978	-2.067057	3.442825
H	3.566474	-0.740385	2.527617
H	2.709269	-2.268511	2.694846
H	2.827472	-2.883520	-2.567047
H	3.693190	-1.359321	-2.725409
H	4.454145	-2.864266	-3.269664
H	7.690346	-4.974952	-0.435668
H	8.400649	-3.540711	0.309408
H	7.646983	-4.772592	1.324778
C	-0.029117	5.457641	-1.072783
C	-0.035268	6.737331	-0.500470
C	-0.039622	6.930770	0.879807
C	-0.033153	5.794095	1.693682
C	-0.026996	4.499270	1.168717
C	-0.024186	5.352620	-2.586315
H	-0.036069	7.604630	-1.157839
C	-0.066030	8.316680	1.481047
H	-0.031925	5.916579	2.775426
C	-0.019726	3.330757	2.129240
H	0.864278	2.698511	1.992829
H	-0.021801	3.685667	3.164515
H	-0.896174	2.688040	1.992980
H	-0.026821	6.349661	-3.037141
H	0.861764	4.827186	-2.964527
H	-0.903958	4.820421	-2.969489
H	0.673588	8.420081	2.283781
H	0.144571	9.083438	0.728500
H	-1.047273	8.544236	1.918108

Triangulene, E_{el} = –845.611885 Hartree

C	2.827647	-2.478299	0.000000
C	2.827647	2.478299	0.000000
C	0.730027	-3.689033	0.000000
C	0.730027	3.689033	0.000000
C	0.710571	-1.233519	0.000000
C	0.710571	1.233519	0.000000
C	2.122598	-3.679240	0.000000
C	2.122598	3.679240	0.000000
C	2.143882	-1.232629	0.000000
C	2.143882	1.232629	0.000000
C	-2.141959	-1.241941	0.000000
C	-2.141959	1.241941	0.000000
C	-0.007029	2.474650	0.000000
C	-0.007029	-2.474650	0.000000
C	-1.426266	0.000000	0.000000
C	2.827857	0.000000	0.000000
C	-4.250127	0.000000	0.000000
C	-0.001840	0.000000	0.000000
C	-3.562793	-1.210959	0.000000
C	-3.562793	1.210959	0.000000
C	-1.416515	-2.450324	0.000000
C	-1.416515	2.450324	0.000000
H	3.915519	0.000000	0.000000
H	-5.336973	0.000000	0.000000
H	0.188706	-4.631692	0.000000
H	0.188706	4.631692	0.000000
H	2.665855	-4.620514	0.000000
H	2.665855	4.620514	0.000000
H	3.914561	2.479737	0.000000
H	3.914561	-2.479737	0.000000
H	-4.108366	-2.151078	0.000000
H	-4.108366	2.151078	0.000000

H	-1.960270	-3.392459	0.000000
H	-1.960270	3.392459	0.000000

Mes$_3$-Tr, E_{el} = –1892.620998 Hartree

C	2.755601	0.761098	-0.000002
C	1.742695	1.760124	0.000001
C	0.358105	1.378489	0.000002
C	0.000061	0.000062	0.000000
C	1.014798	-0.999227	-0.000004
C	2.398989	-0.616176	-0.000005
C	3.387510	-1.638350	-0.000009
C	3.027339	-2.981174	-0.000012
C	1.690198	-3.361865	-0.000010
C	0.653007	-2.389135	-0.000005
C	-1.372715	-0.379078	0.000001
C	-1.733075	-1.769347	0.000000
C	-0.718628	-2.766819	-0.000002
C	-3.112555	-2.114364	0.000002
C	-4.095396	-1.131043	0.000004
C	-3.756524	0.217306	0.000004
C	-2.395522	0.629195	0.000003
C	-0.665723	2.385711	0.000004
C	-2.036783	2.005914	0.000003
C	2.066497	3.144731	0.000003
C	1.068233	4.112383	0.000006
C	-0.274770	3.752884	0.000006
C	-1.095428	-4.218325	0.000000
H	1.341488	5.164445	0.000007
H	-4.533151	0.974049	0.000005
H	4.434276	-1.355315	-0.000011
H	-5.143135	-1.420433	0.000005
H	3.801825	-3.743851	-0.000016
H	1.423122	-4.412809	-0.000012

H	-3.390799	-3.162417	0.000002
H	-1.043289	4.517878	0.000007
H	3.110174	3.438933	0.000003
C	-3.105477	3.057928	0.000001
C	4.201040	1.160527	-0.000001
C	-1.275888	-4.903413	-1.220747
C	-1.630988	-6.256252	-1.197735
C	-1.810434	-6.953590	0.000005
C	-1.630975	-6.256251	1.197742
C	-1.275874	-4.903413	1.220749
C	-1.095015	-4.194708	-2.544652
H	-1.772067	-6.777477	-2.142921
C	-2.162616	-8.423208	0.000007
H	-1.772043	-6.777476	2.142929
C	-1.094987	-4.194708	2.544652
C	4.884563	1.346795	1.220749
C	6.233711	1.715659	1.197742
C	6.927351	1.908905	0.000001
C	6.233713	1.715658	-1.197741
C	4.884565	1.346794	-1.220750
C	4.180317	1.149187	2.544640
H	6.755647	1.854083	2.142928
C	8.376182	2.338674	0.000002
H	6.755650	1.854082	-2.142927
C	4.180321	1.149185	-2.544642
C	-3.608657	3.556638	-1.220748
C	-4.602980	4.540300	-1.197743
C	-5.117333	5.044209	-0.000004
C	-4.602982	4.540303	1.197738
C	-3.608659	3.556642	1.220748
C	-3.085144	3.045809	-2.544638
H	-4.983936	4.922984	-2.142930
C	-6.214295	6.083672	-0.000006

H	-4.983940	4.922990	2.142923
C	-3.085148	3.045817	2.544641
H	-2.745529	-8.696117	0.886307
H	-2.745553	-8.696114	-0.886279
H	-1.260221	-9.049546	-0.000007
H	-1.273549	-4.877889	-3.380814
H	-1.785003	-3.348718	-2.646009
H	-0.081297	-3.790341	-2.649080
H	-1.784971	-3.348714	2.646014
H	-1.273516	-4.877887	3.380816
H	-0.081266	-3.790344	2.649070
H	8.903981	1.970279	-0.886288
H	8.467443	3.433337	-0.000005
H	8.903976	1.970290	0.886299
H	3.792039	0.128863	-2.645780
H	3.323683	1.825412	-2.649252
H	4.861382	1.335570	-3.380820
H	4.861378	1.335569	3.380819
H	3.323681	1.825415	2.649250
H	3.792032	0.128866	2.645777
H	-6.159373	6.724982	0.886279
H	-6.159389	6.724961	-0.886308
H	-7.207770	5.615032	0.000008
H	-2.007586	3.220869	2.646020
H	-3.587772	3.541753	3.380819
H	-3.241304	1.965649	2.649004
H	-3.587764	3.541744	-3.380819
H	-2.007582	3.220856	-2.646015
H	-3.241304	1.965641	-2.649000

S9. References

1 P. Ribar, L. Valenta, T. Šolomek and M. Juríček, *Angew. Chem. Int. Ed.*, 2021, **60**, 13521–13528.

2 C. J. Holt, K. J. Wentworth and R. P. Johnson, *Angew. Chem. Int. Ed.*, 2019, **58**, 15793–15796.

3 Y. Gu, X. Wu, T. Y. Gopalakrishna, H. Phan and J. Wu, *Angew. Chem. Int. Ed.*, 2018, **57**, 6541–6545.

4 L. A. van de Kuil, H. Luitjes, D. M. Grove, J. W. Zwikker, J. G. M. van der Linden, A. M. Roelofsen, L. W. Jenneskens, W. Drenth and G. van Koten, *Organometallics*, 1994, **13**, 468–477.

5 G. R. Fulmer, A. J. M. Miller, N. H. Sherden, H. E. Gottlieb, A. Nudelman, B. M. Stoltz, J. E. Bercaw and K. I. Goldberg, *Organometallics*, 2010, **29**, 2176–2179.

6 G.-Q. Li, Y. Yamamoto and N. Miyaura, *Synlett*, 2011, **2011**, 1769–1773.

7 T. J. Boyd and R. R. Schrock, *Macromolecules*, 1999, **32**, 6608–6618.

8 R. C. Clark and J. S. Reid, *Acta Crystallogr. Sect. A*, 1995, **51**, 887–897.

9 R. O. D. Ltd, CrysAlisPro (Version 1.171.40.68a). Yarnton, Oxfordshire, England 2019.

10 O. V Dolomanov, L. J. Bourhis, R. J. Gildea, J. A. K. Howard and H. Puschmann, *J. Appl. Crystallogr.*, 2009, **42**, 339–341.

11 G. M. Sheldrick, *Acta Crystallogr. Sect. A*, 2015, **71**, 3–8.

12 G. M. Sheldrick, *Acta Crystallogr. Sect. C*, 2015, **71**, 3–8.

13 A. L. Spek, *Acta Crystallogr. Sect. D*, 2009, **65**, 148–155.

14 A. L. Spek, *Acta Crystallogr. Sect. C*, 2015, **71**, 9–18.

15 K. Herb, R. Tschaggelar, G. Denninger and G. Jeschke, *J. Magn. Reson.*, 2018, **289**, 100–106.

16 R. Improta and V. Barone, *Chem. Rev.*, 2004, **104**, 1231–1254.

17 Gaussian 09, Revision D.01, M. J. Frisch, G. W. Trucks, H. B. Schlegel, G. E. Scuseria, M.A. Robb, J. R. Cheeseman, G. Scalmani, V. Barone, B. Mennucci, G. A. Petersson, H.Nakatsuji, M. Caricato, X. Li, H. P. Hratchian, A. F. Izmaylov, J. Bloino, G. Zheng, J. L.Sonnenberg, M. Hada, M. Ehara, K. Toyota, R. Fukuda, J. Hasegawa, M. Ishida, T.Nakajima, Y. Honda, O. Kitao, H. Nakai, T. Vreven, J. A. Montgomery, Jr., J. E. Peralta, F.Ogliaro, M. Bearpark, J. J. Heyd, E. Brothers, K. N. Kudin, V. N. Staroverov, R.Kobayashi, J. Normand, K. Raghavachari, A. Rendell, J. C. Burant, S. S. Iyengar, J.Tomasi, M. Cossi, N. Rega, J. M. Millam, M. Klene, J. E. Knox, J. B. Cross, V. Bakken, C.Adamo, J. Jaramillo, R. Gomperts, R. E. Stratmann, O. Yazyev, A. J. Austin, R. Cammi, C.Pomelli, J. W. Ochterski, R. L. Martin, K. Morokuma, V. G. Zakrzewski, G. A. Voth, P.Salvador, J. J. Dannenberg, S. Dapprich, A. D. Daniels, Ö. Farkas, J. B. Foresman, J. V.Ortiz, J. Cioslowski, and D. J. Fox, Gaussian, Inc., Wallingford CT, 2009.

18 P. Ribar, T. Šolomek and M. Juríček, *Org. Lett.*, 2019, **21**, 7124–7128.

19 F. Neese, *WIREs Comput. Mol. Sci.*, 2018, **8**, e1327.

20 K. Yamaguchi, H. Fukui and T. Fueno, *Chem. Lett.*, 1986, **15**, 625–628.

21 M. Nishino, S. Yamanaka, Y. Yoshioka and K. Yamaguchi, *J. Phys. Chem. A*, 1997, **101**, 705–712.

22 A. Das, T. Müller, F. Plasser and H. Lischka, *J. Phys. Chem. A*, 2016, **120**, 1625–1636.